AN ABSTRACT OF THE THESIS OF

Chung-Yi Shen (Name) for the M.S. (Degree) in Mechanical Engineering (Major)

Date thesis is presented May 14, 1963

Title THE DISTRIBUTION OF MOISTURE CONDENSED FROM SATURATED AIR FLOWING THROUGH COOLED POROUS MEDIA

Abstract approved [redacted]
(Major professor)

A theoretical study of the heat and mass transfer between saturated air and a cooled porous bed is made and experimental verification is presented.

It is shown by the analysis that the parameter, $\frac{nGC_p}{\overline{K}}L$, has the most effect upon the shape of the temperature distribution. When the value of $\frac{nGC_p}{\overline{K}}L$ exceeds 10, the temperature of the air-water vapor mixture drops very little at the beginning portion of the porous bed and decreases rapidly toward the end next to the heat exchanger. When the value of $\frac{nGC_p}{\overline{K}}L$ becomes smaller, the temperature distribution becomes more linear. The pressure distribution is nearly linear and depends slightly on the temperature distribution. Both calculated and experimental results show that the moisture distribution approaches to uniform distribution when the value of $\frac{nGC_p}{\overline{K}}L$ is equal to 0.30.

The qualitative agreement between the experimental results and the theoretical prediction is good. The quantitative agreement of temperature, pressure, and moisture distribution is within 10 to 20%. Most of the discrepancy is the result of the following factors:

1. Information on how the thermal conductivity of different porous beds varies with moisture content is not available.
2. The thermal conductivity of the porous bed is not uniform due to the nonuniform distribution of moisture.
3. The compaction of the porous bed is not uniform. Consequently, a nonuniform distribution of flow results.

THE DISTRIBUTION OF MOISTURE CONDENSED FROM SATURATED AIR FLOWING THROUGH COOLED POROUS MEDIA

by

CHUNG-YI SHEN

A THESIS

submitted to

OREGON STATE UNIVERSITY

in partial fulfillment of
the requirements for the
degree of

MASTER OF SCIENCE

June 1963

APPROVED:

[redacted]

Associate Professor of Mechanical Engineering

In Charge of Major

[redacted]

Head of Department of Mechanical Engineering

[redacted]

Dean of Graduate School

Date thesis is presented May 14, 1963

Typed by Carol Baker

ACKNOWLEDGEMENT

The author wishes to express his appreciation to the National Science Foundation for the research assistantship which made this study possible. To Dr. Milton B. Larson, the author wishes to express thankful appreciation for his sincere interest, advice, and suggestions in pursuing this problem and in preparation of this thesis. Many helpful suggestions were obtained from Dr. John W. Wolfe. Many thanks are given to Mr. John E. Postlewaite for his help in the experimental work.

TABLE OF CONTENTS

LIST OF FIGURES

LIST OF TABLES

NOMENCLATURE

A	Cross-sectional area of test section, ft^2
$\dot{B}$	Energy generated per unit volume due to heat of wetting, $BTU/ft^3\text{-}sec$
C_p	Specific heat at constant pressure of dry air, BTU/lb-F
D_p	Effective particle diameter, ft
D_v	Diffusivity of gas, ft^2/hr
e	Internal energy of the mixture of air and water vapor, BTU/lb
e_f	Internal energy of condensed liquid, BTU/lb
e_s	Internal energy of solid particles, BTU/lb
f	Porosity, void volume/total volume
G	Mass flow rate of dry air, $lb/hr\text{-}ft^2$
h	Local film coefficient, $BTU/ft^2\text{-}F\text{-}hr$
i	Enthalpy of the mixture of air and water vapor, BTU/lb
i_a	Enthalpy of the dry air, BTU/lb
i_f	Enthalpy of the condensed liquid, BTU/lb
i_v	Enthalpy of the water vapor, BTU/lb
$\dot{J}$	Transfer factor
K	Thermal conductivity of the porous bed, BTU/ft-F-hr
K_f	Thermal conductivity of the condensed liquid, BTU/ft-F-hr
K_s	Thermal conductivity of the solid, BTU/ft-F-hr
k	Thermal conductivity of the gas, BTU/ft-F-hr
k_g	Thermal conductivity of gas film, $lb\text{-}moles/hr\text{-}ft^2\text{-}atm.$

L	Thickness of the porous bed, ft
M_m	Mean molecular weight of gas stream
P	Total pressure of the mixture of air and vapor, lb/ft^2
P_a	Partial pressure of the dry air, lb/ft^2
P_v	Partial pressure of the water vapor, lb/ft^2
P_{f_g}	Log mean partial pressure of the non-transferred gases in the gas film
q	Rate of heat flow, BTU/hr
R	Radius of average particle, ft
R_a	Gas constant of dry air, ft-lb/°R
S	Specific surface, surface area of particle/unit volume, ft^2/ft^3
T	Temperature of the mixture of air and vapor, °F
t	Temperature of the solid particles and liquid film, °F
V	Average velocity of saturated air in x direction, ft/sec
$\dot{W}_c$	Rate of moisture condensed per unit volume, lb/ft^3-sec
$\dot{W}_r$	Rate of moisture removed per unit volume, lb/ft^3-sec
x	Distance, ft
$\frac{C_p\mu}{k}$	Prandtl number
$\frac{D_pG}{k}$	Reynolds number
$\frac{\mu}{\rho D_v}$	Schmidt number
ρ	Density of the mixture of air and vapor, lb/ft^3
ρ_a	Density of the dry air, lb/ft^3

ρ_v Density of the vapor, lb/ft^3

ρ_q Bulk density of quartz sand, lb/ft^3

ρ_s Bulk density of solid particles, lb/ft^3

ω Specific humidity, mass of water vapor/mass of dry air

μ Viscosity of the gas, lb/hr-ft

ϕ Permeability of the porous bed, Darcy

δ Thickness of liquid film, ft

θ Time, sec

Θ Total operation time, hr

$\simeq$ Approximately equal sign

$\sim$ Proportional sign

THE DISTRIBUTION OF MOISTURE CONDENSED FROM SATURATED AIR FLOWING THROUGH COOLED POROUS MEDIA

INTRODUCTION

Methods for applying moisture uniformly to soils have been investigated by many research workers during the past. But, at a moisture content well below the field capacity, no successful method has been developed. John Wolfe (9), in his Ph. D. dissertation, investigated the possibility of achieving this goal by means of vapor irrigation. His method was to force saturated air through a soil column, 3-inches deep and 4-inches square, while the temperature of the soil was controlled by five grills which were equally spaced in the soil column. The temperatures of these grills were calculated on the basis of a linear pressure distribution and a constant rate of change of specific humidity with distance along the flow path. Although perfect uniformity of moisture distribution was not attained, the results from his work indicated that this was a promising approach.

The present study was an extension of Wolfe's investigation. Instead of using grills to control the soil temperature, one side of the soil column was cooled to a constant temperature while warm saturated air was allowed to enter through the opposite side. The operating temperature in the soil was generally between 60° and 80° F, and the maximum pressure drop across the soil column did not

exceed 5 psi. Besides the soil, fine glass beads, and a mixture of glass beads and chrome powder were also used. A theoretical analysis and an experimental verification have been made and presented.

At the same time, John Postlewaite (10) has studied the problem to determine the conditions required for spacewise uniform condensation from saturated air flowing through cooled porous media.

REVIEW OF LITERATURE

In 1943, Wilke and Hougen (8) experimentally evaluated friction factors, film coefficients, and mass transfer coefficients for flow of gases through granular solids. Their results indicated that for laminar flow, $N_{Re} < 40$,

$$\dot{J}_h = 18.1 \left(\frac{D_p G}{\mu}\right)^{-1}$$

and

$$\dot{J}_d = 16.8 \left(\frac{D_p G}{\mu}\right)^{-1}$$

where

$$\dot{J}_h = \frac{h}{C_p G} \left(\frac{C_p \mu}{k}\right)^{2/3}_f$$

and

$$\dot{J}_d = \frac{k_g P_{fg} M_m}{G} \left(\frac{\mu}{\rho D_v}\right)^{2/3}_f .$$

The subscript f refers to the properties of gas film. It was also observed that for all conditions of flow, turbulent, laminar or transition, the ratio of $\dot{J}_h$ and $\dot{J}_d$ remained constant, that is

$$\frac{\dot{J}_h}{\dot{J}_d} = 1.076.$$

In 1945, more data were obtained in the low Reynolds number region,

and the expression

$$\dot{J}_d = 16.8 \left(\frac{D_p G}{\mu}\right)^{-1}$$

was revised to a more reliable value

$$\dot{J}_d = 1.82 \left(\frac{D_p G}{\mu}\right)^{-0.51} .$$

No information was given on the value of $\dot{J}_h$. It is assumed here that the ratio $\dot{J}_h$ to $\dot{J}_d$ is unchanged.

Weinbaum and Wheller (7) formed an analysis of heat transfer inside sweat-cooled metals. The temperature distributions along the length of a sweat-cooled bar and through a sweat-cooled hollow cylinder were obtained. For the sweat-cooled bar, the temperature of the metal and the fluid are indistinguishable throughout most of the thickness of the metal. This same topic is also considered in Schneider's Conduction Heat Transfer (5).

More discussion of heat transfer from fluidized and packed beds is given in McAdam's Heat Transmission (4). The flow of fluids through porous media is thoroughly treated in Muskat's Flow of Homogeneous Fluids (3) and Scheidergger's The Physics of Flow Through Porous Media (6). Many physical aspects of soil such as the heat of wetting and the dependence of thermal conductivity on moisture content are discussed in Baver's Soil Physics (1).

DEVELOPMENT OF GOVERNING DIFFERENTIAL EQUATIONS

A porous bed of thickness L is contained within an insulated, circular cylinder and is fixed in place by fine wire screens at each end. The temperature of the bed at x=L is t_L, and the temperature of incoming saturated air at x=0 is T_0. The porous bed will be assumed to be a continuum, and the mixture of air and water vapor will be treated as a perfect gas. Condensed liquid may be partly absorbed by the solid particles and the rest will form a liquid film around each particle. Since $K_f \simeq K_S$, and $\frac{\delta}{R} \ll 1$ for sandy soil or glass beads, the temperature of liquid film will be approximately the same as that of the solid particle (dotted line in Figure 2). Also it is assumed that there will be no movement of either the condensed liquid or the solid particles.

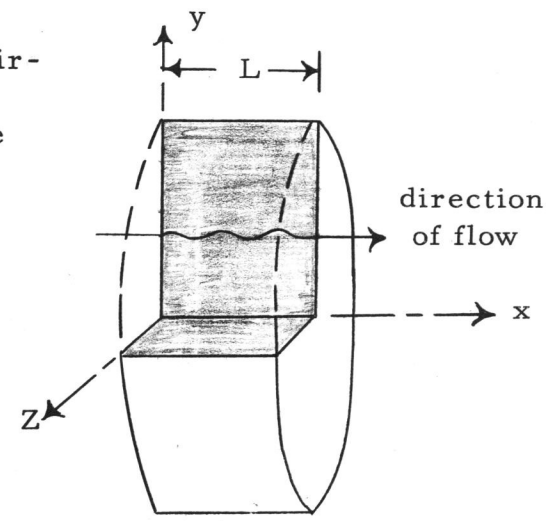

Figure 1. Model of a porous bed.

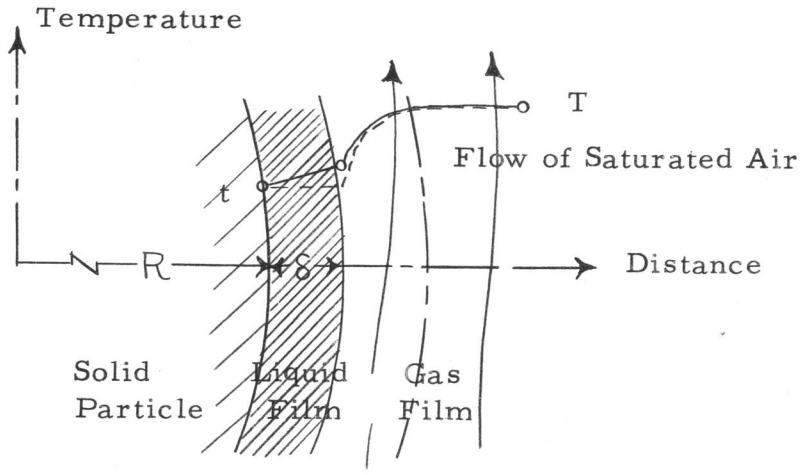

Figure 2. Temperature profile of saturated air and solid particle.

Consider a differential element as shown by Figure 3 which consists of solid particles, condensed liquid, and saturated air. For purposes of analysis the element is further divided into two control volumes:

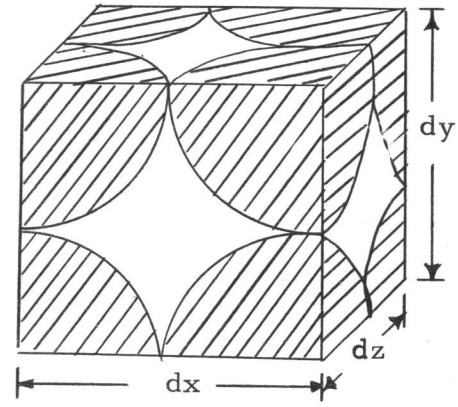

Figure 3. Differential Element.

1. Air-vapor control volume
2. Solid-liquid control volume

The air-vapor control volume will consist of the pore volume which contains the air and water vapor. Any liquid within the differential element is considered to lie outside this control volume. The solid-liquid control volume will consist of the solid particles and the condensed liquid.

The principles of conservation of mass, as applied to the

air-vapor control volume requires that

$$\rho V dydz = [\rho V + \frac{\partial}{\partial x}(\rho V)dx]dydz + \dot{W}_c dxdydz + \frac{\partial}{\partial \theta}(f\rho)dxdydz$$

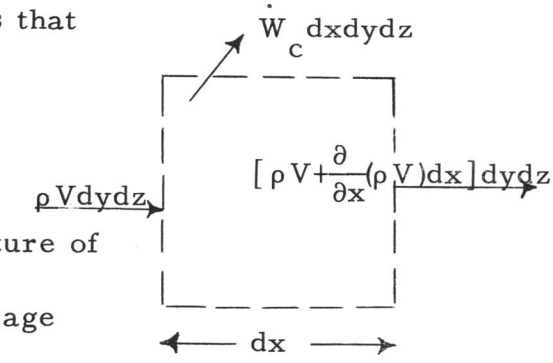

Figure 4. Mass flux in and out of air-vapor control volume

where ρ is the density of the mixture of air and water vapor, V is the average velocity in the x direction, $\dot{W}_c$ is the rate of moisture condensation per unit volume, f is the porosity, and θ is the time. Upon cancelling equal terms and dividing by dx dy dz this becomes

$$\frac{\partial}{\partial x}(\rho V) + \dot{W}_c = \frac{\partial}{\partial \theta}(f\rho). \qquad (1)$$

The same principle applied to solid-liquid control volume requires that

$$\dot{W}_c dxdydz = \dot{W}_r dxdydz + \frac{\partial \rho_f}{\partial \theta} dxdydz$$

where $\dot{W}_r$ is the rate of moisture removed per unit volume, and ρ_f is the density of condensed liquid defined as the mass of the liquid divided by the total volume. Divided by dx dy dz, the above expression becomes

$$\dot{W}_c = \dot{W}_r + \frac{\partial \rho_f}{\partial \theta}. \qquad (2)$$

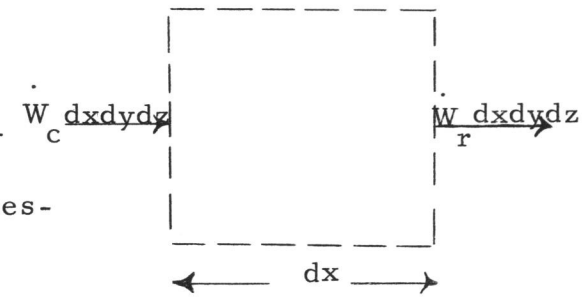

Figure 5. Mass flux of condensate in and out of solid-liquid control volume.

The momentum equation for flow through porous media is given by Darcy's law which has been established by experiment. It states that at low Reynolds number, the velocity varies linearly with the pressure gradient.

$$V = -\frac{\phi}{\mu}\frac{\partial P}{\partial x} \tag{3}$$

where ϕ is the permeability of the porous medium and μ is the viscosity of the fluid. This empirical law has been accepted as a foundation for the study of flow through porous media.

The principle of conservation of energy requires that:

The rate of energy in-flow = The rate of energy out-flow + The rate of change of storage of energy.

For air-vapor control volume, the rate of enthalpy flow into the control volume is

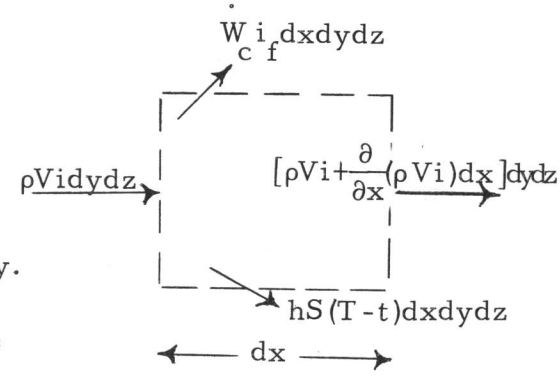

Figure 6. Energy flux in and out of air-vapor control volume.

$$\rho Vidydz$$

where i is the enthalpy of the mixture of air and vapor. The rate of enthalpy flow out of the control volume is

$$[\rho Vi + \frac{\partial}{\partial x}(\rho Vi)dx]dydz.$$

The heat transfer into the solid-liquid control volume by convection is

$$hS(T-t)dxdydz$$

where h is the local film coefficient, S is the specific surface, T is the temperature of the saturated air, and t is the temperature of solid particles and liquid film. The energy added to the solid-liquid control volume because of condensation is

$$\dot{W}_c i_f dxdydz$$

where i_f is the enthalpy of condensed liquid. The rate of change of energy storage within the control volume is

$$\frac{\partial}{\partial \theta}(f\rho e)dxdydz$$

where e is the internal energy of the mixture of air and water vapor. Substituting all the terms into the above expression will give

$$\rho Vidydz = [\rho Vi + \frac{\partial}{\partial x}(\rho V_i)dx]dydz + hS(T-t)dxdydz + \dot{W}_c i_f dxdydz + \frac{\partial}{\partial \theta}(f\rho e)dxdydz .$$

Combining the terms and dividing by $dx\,dy\,dz$ gives

$$\frac{\partial}{\partial x}(\rho Vi) + hS(T-t) + \dot{W}_c i_f = -\frac{\partial}{\partial \theta}(f\rho e) . \qquad (4)$$

Before writing the energy equation for the solid-liquid control volume, a special phenomenon which the soil possesses during wetting must be examined. This is called the heat of wetting. Essentially, it represents the loss in kinetic energy of water

molecules during absorption by the solid particles. The amount of heat of wetting generally depends on the type of soil and the soil moisture content (Figure 7). For glass beads and sandy soil, the heat of wetting can be neglected.

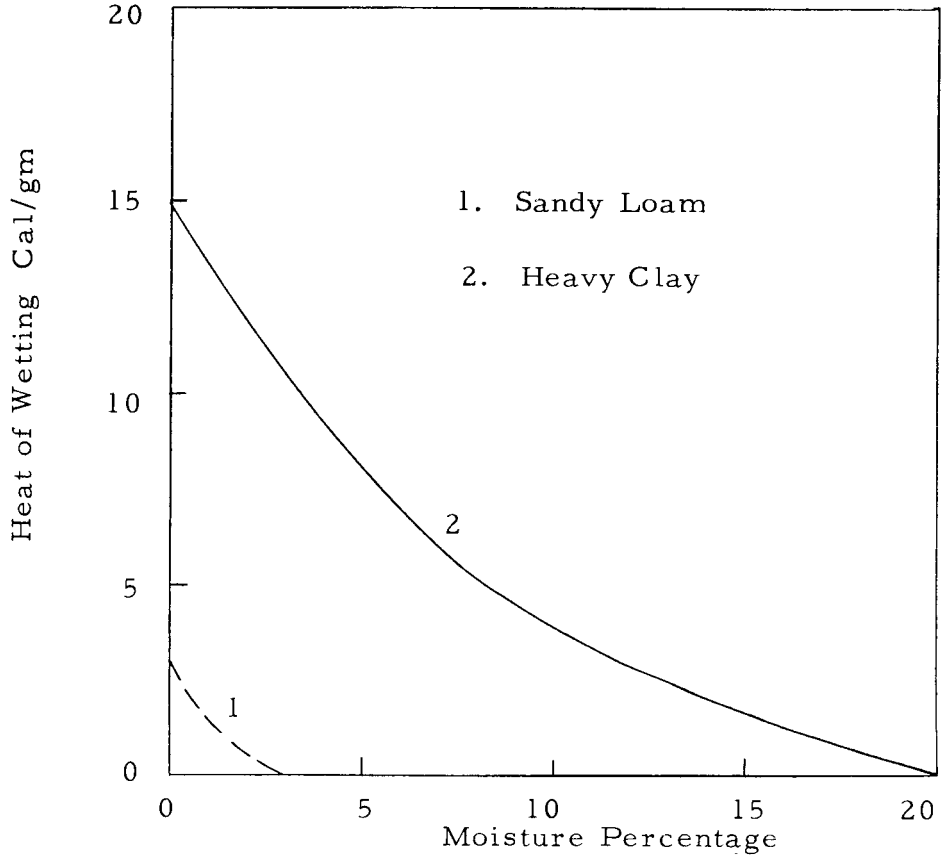

Figure 7. Heat of wetting for two types of soil
(p. 44 Baver's Soil Physics)

Applying the principle of conservation of energy to the solid-liquid control volume will give

$$-K\frac{\partial t}{\partial x}dydz + hS(T-t)dxdydz$$

$$+\dot{B}\,dxdydz + \dot{W}_c i_f\,dxdydz$$

$$= -\left[K\frac{\partial t}{\partial x} + \frac{\partial}{\partial x}\left(K\frac{\partial t}{\partial x}\right)dx\right]dydz$$

$$+ \dot{W}_r i_f dxdydz + \frac{\partial}{\partial \theta}(\rho_s e_s + \rho_f e_f)dxdydz\ .$$

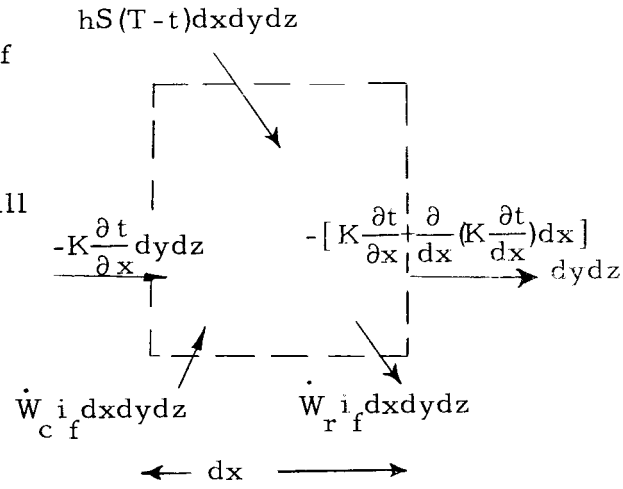

Figure 8. Energy flux in and out of the solid-liquid control volume.

The term, $-K\frac{\partial t}{\partial x}dydz$, is the heat conducted through the face at x of the solid-liquid control volume, and the term $-\left[K\frac{\partial t}{\partial x}+\frac{\partial}{\partial x}\left(K\frac{\partial t}{\partial x}\right)dx\right]dydz$, is the heat conducted through the face at x + dx. $\dot{B}$ is the rate of energy "generated" per unit volume which accounts for the heat of wetting. ρ_s is the bulk density of solid particles, e_s is the internal energy of solid particles and e_f is the internal energy of condensed liquid. Simplifying the above equation gives

$$\frac{\partial}{\partial x}\left(K\frac{\partial t}{\partial x}\right) + hS(T-t) + \dot{B} + i_f(\dot{W}_c - \dot{W}_r) = \frac{\partial}{\partial \theta}(\rho_s e_s + \rho_f e_f). \quad (5)$$

QUASI-STEADY STATE SOLUTION

The partial differential equations which have been developed in the preceeding section are summarized below:

1. $\frac{\partial}{\partial x}(\rho V) + \dot{W}_c = -\frac{\partial}{\partial \theta}(f\rho)$

2. $\dot{W}_c = \dot{W}_r + \frac{\partial \rho_f}{\partial \theta}$

3. $V = -\frac{\phi}{\mu}\frac{\partial p}{\partial x}$

4. $\frac{\partial}{\partial x}(\rho V i) + hS(T-t) + \dot{W}_c i_f = -\frac{\partial}{\partial \theta}(f\rho e)$

5. $\frac{\partial}{\partial x}(K\frac{\partial t}{\partial x}) + hS(T-t) + i_f(\dot{W}_c - \dot{W}_r) + \dot{B} = \frac{\partial}{\partial \theta}(\rho_s e_s + \rho_f e_f)$

Because ρ_s is a constant, the right hand side of equation 5 may be written as

$$\rho_s \frac{\partial e_s}{\partial \theta} + \rho_f \frac{\partial e_f}{\partial \theta} + e_f \frac{\partial \rho_f}{\partial \theta} \quad .$$

Using equation 2 to eliminate $\frac{\partial \rho_f}{\partial \theta}$ will reduce this to

$$\rho_s \frac{\partial e_s}{\partial \theta} + \rho_f \frac{\partial e_f}{\partial \theta} + e_f (\dot{W}_c - \dot{W}_r) \quad .$$

Since the enthalpy of saturated liquid is approximately the same as the internal energy, equation 5 becomes

$$\frac{\partial}{\partial x}\left(K \frac{\partial t}{\partial x}\right) + hS\ (T-t) + \dot{B} = \rho_s \frac{\partial e_s}{\partial \theta} + \rho_f \frac{\partial e_f}{\partial \theta} \quad .$$

Furthermore, $\dot{W}_r$ and $\dot{B}$ can be assumed to be zero if glass beads or sandy soil is used and if no condensed moisture is removed.

Even with the simplifications made above, these partial differential equations are still very difficult to solve. As an approximation, a transient problem can be treated as a steady state problem in a period of time during which changes are small. This quasi-steady state will be considered here.

If temperature, pressure, and moisture content in the porous bed change slowly with time, then the terms, $\frac{\partial}{\partial \theta}(f\rho)$, $\frac{\partial}{\partial \theta}(f\rho e)$, $\frac{\partial e_f}{\partial \theta}$, and $\frac{\partial e_s}{\partial \theta}$ become negligible. Using these approximations, the above equations become:

7. $\frac{d}{dx}(\rho V) + \dot{W}_c \simeq 0$

8. $V \simeq - \frac{\phi}{\mu} \frac{dp}{dx}$

9. $\frac{d}{dx}(\rho V i) + \bar{h}S\ (T-t) + \dot{W}_c i_f \simeq 0$

10. $\bar{K} \frac{d^2 t}{dx^2} + \bar{h}S\ (T-t) \simeq 0$

where $\bar{h}$ is the average film coefficient and $\bar{K}$ is the average thermal conductivity of the porous bed.

Since the flow is a mixture of air and water vapor, equation 7 can be written as

$$\frac{d}{dx}(\rho_a V + \rho_v V) + \dot{W}_c = 0. \tag{11}$$

But,

$$\frac{d}{dx}(\rho_a V) = 0 \tag{12}$$

or

$$\rho_a V = G$$

where G is a constant. Hence,

$$\frac{d}{dx}(\rho_v V) + \dot{W}_c = 0 \tag{13}$$

Using equation 8 to eliminate V from equation 12 gives

$$\frac{d}{dx}\left[\rho_a\left(-\frac{\phi}{\mu}\frac{dp}{dx}\right)\right] = 0. \tag{14}$$

Using the perfect gas law and the relation, $P = P_a + P_v$, equation 14 can be written as

$$-\frac{d}{dx}\left[\frac{P_a}{R_a T}\frac{\phi}{\mu}\frac{d(P_a+P_v)}{dx}\right] = 0$$

or

$$\frac{d}{dx}\left[\frac{P_a}{R_a T}\frac{\phi}{\mu}\frac{dP_a\left(1+\frac{P_v}{P_a}\right)}{dx}\right] = 0 .$$

Integrating once with respect to x will give

$$\frac{P_a}{R_a T}\frac{\phi}{\mu}\frac{d}{dx}P_a\left(1+\frac{P_v}{P_a}\right) = C_1$$

where C_1 is the integration constant. Since $P_v << P_a$, $\frac{P_v}{P_a}$ will be much smaller than 1. For a good approximation, it can be neglected, and the above expression becomes

$$P_a \frac{dP_a}{dx} = C_1 \frac{\mu}{\phi} R_a T$$

or

$$\frac{dP_a^2}{dx} = 2 C_1 \frac{\mu}{\phi} R_a T .$$

If μ and ϕ are assumed to be constant, the above expression can be integrated as follows:

$$P_a^2 = C_2 \int T \, dx + C_3 \qquad (15)$$

where C_2 is equal to $2C_1 \frac{\mu}{\phi} R_a$, and C_3 is the integration constant. Both C_2 and C_3 can be determined by the following boundary conditions:

1. $P = P_0$ when $x = 0$
2. $P = P_L$ when $x = L$

From equation 15, it is clear that the pressure distribution will depend upon the temperature distribution. It is expected that the temperature distribution of the air-water vapor mixture will lie somewhere between a linear temperature distribution and a constant temperature at the inlet temperature. Therefore, the corresponding pressure distribution for these two cases can be calculated by using

equation 15. For a temperature difference of 20°F and a total pressure drop of 5 psi across the porous column, the difference in pressure distribution between the linear temperature distribution and the constant temperature distribution is less than 2%, and the maximum deviation from the linear pressure distribution for both cases is less than 8% (Figure 9). For simplicity, the pressure distribution will be assumed to be linear.

Since $\rho_a V = G$, and $\frac{\rho_v}{\rho_a} = \omega$, equation 13 can be written as

$$G\frac{d\omega}{dx} + \dot{W}_c = 0. \tag{16}$$

By using the relation, $\rho i = \rho_a i_a + \rho_v i_v$, equation 9 becomes

$$\frac{d}{dx}(\rho_a V i_a) + \frac{d}{dx}(\rho_v V i_v) + \bar{h}S(T-t) + \dot{W}_c i_f = 0$$

or

$$GC_p\frac{dT}{dx} + i_v\frac{d}{dx}(\rho_v V) + \rho_v V\frac{di_v}{dx} + \bar{h}S(T-t) + \dot{W}_c i_f = 0$$

where i_v can be treated as a constant within a small range of temperature. Using equation 16, the above expression becomes

$$GC_p\frac{dT}{dx} + G(i_v - i_f)\frac{d\omega}{dx} + \bar{h}S(T-t) = 0. \tag{17}$$

Solving for t gives

$$t = \frac{GC_p}{\bar{h}S}\frac{dT}{dx} + \frac{Gi_{vf}}{\bar{h}S}\frac{d\omega}{dx} + T. \tag{18}$$

Differentiating it twice with respect to x, and substituting into

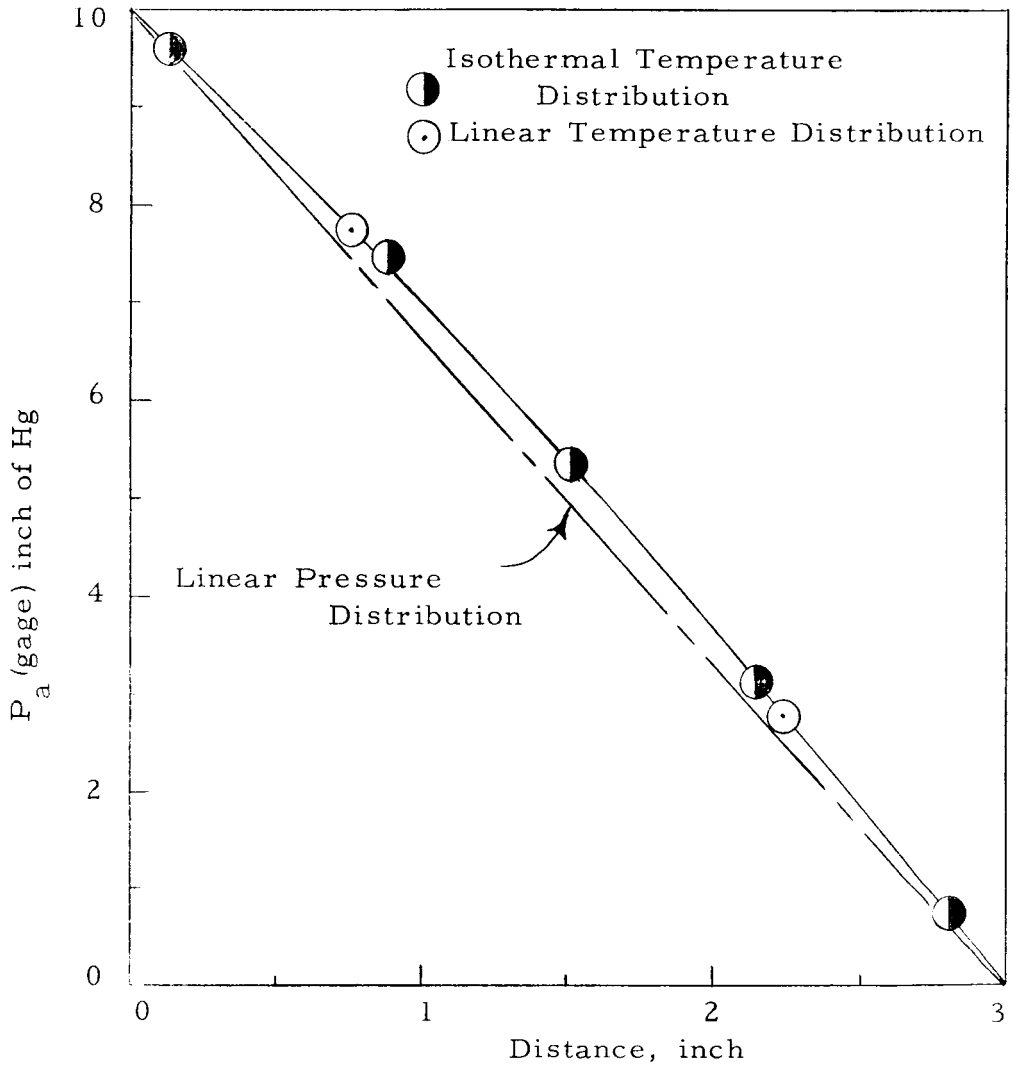

Figure 9. Pressure distribution assuming linear or constant temperature distributions

equation 10 will yield

$$\bar{K}\left[\frac{GC_p}{\bar{h}S}\frac{d^3T}{dx^3} + \frac{Gi_{vf}}{\bar{h}S}\frac{d^3\omega}{dx^3} + \frac{d^2T}{dx^2}\right] + \bar{h}S(T-t) = 0.$$

The term, $\bar{h}S\,(T-t)$, can be eliminated by using equation 17 to give

$$\bar{K}\left[\frac{GC_p}{\bar{h}S}\frac{d^3T}{dx^3} + \frac{Gi_{vf}}{\bar{h}S}\frac{d^3\omega}{dx^3} + \frac{d^2T}{dx^2}\right] - GC_p\frac{dT}{dx} - i_{vf}G\frac{d\omega}{dx} = 0.$$

Dividing the above expression by $\bar{K}\dfrac{GC_p}{\bar{h}S}$ gives

$$\frac{d^3T}{dx^3} + \frac{\bar{h}S}{GC_p}\frac{d^2T}{dx^2} - \frac{\bar{h}S}{\bar{K}}\frac{dT}{dx} + \frac{i_{vf}}{C_p}\frac{d^3\omega}{dx^3} - \frac{i_{vf}\bar{h}S}{\bar{K}C_p}\frac{d\omega}{dx} = 0. \quad (19)$$

In order to solve equation 19, a relationship between ω and T is needed. It is known that

$$\omega = 0.622\,\frac{P_v}{P_a} \quad . \quad (20)$$

By the previous assumption of a linear pressure drop, and $P \simeq P_a$, P_a can be written in the form of $C_1x + C_2$ where C_1 and C_2 are arbitrary constants. The moistened air is assumed to be saturated before entering the porous column. If it remains saturated throughout the length of the porous column, then P_v will be a function of temperature only. For a temperature interval of 20°F, P_v can be approximated by a linear relationship. Hence, ω can be expressed in the form:

$$\omega = \frac{C_3 T + C_4}{C_1 x + C_2} \tag{21}$$

where C_3 and C_4 are constants. Substituting equation 21 into equation 19 will give a linear differential equation with variable coefficients. However, the saturated air expands gradually from higher pressure to atmospheric pressure while it flows through the porous column. Therefore, in order to maintain saturation, a minimum temperature distribution is required. To illustrate this point, three arbitrary pressure distributions have been chosen (Figure 10) and the inlet saturated air temperature has been assumed to be 80°F. Hence, the initial specific humidity can be calculated. To maintain the initial specific humidity constant throughout the whole porous column, the value of P_v varies according to equation 20. By using steam table data (2), the corresponding temperature can be determined (Figure 11). Any time that the actual temperature distribution is higher than the minimum required temperature distribution, the air is unsaturated. Since the actual temperature distribution is not known, it is unfounded to say that the air remains saturated throughout the porous column. Hence, P_v cannot be assumed to be a function of temperature only. As will be shown later, for small pressure drop it is reasonable to use the approximation that

$$\frac{d\omega}{dx} \sim \frac{dT}{dx}$$

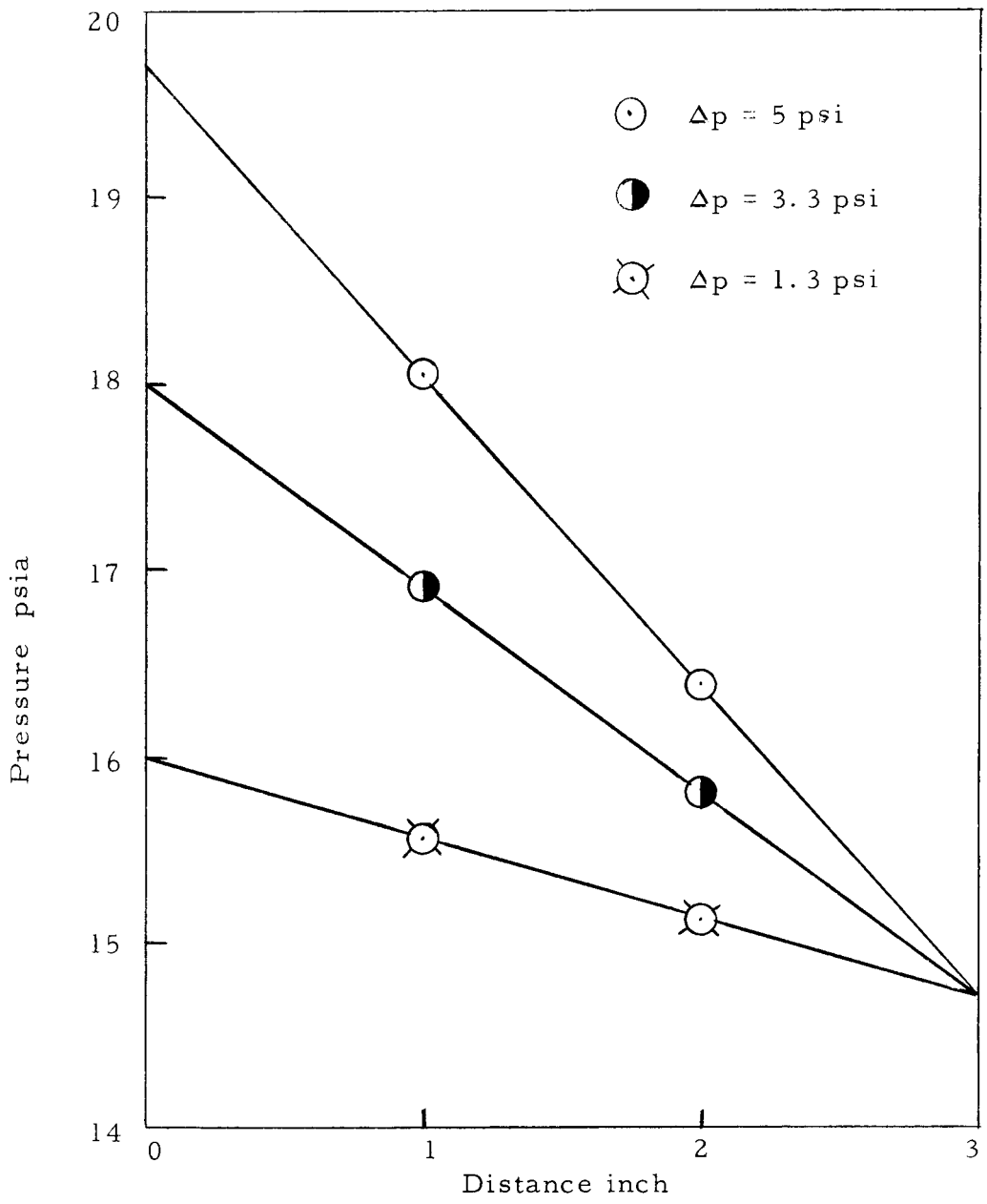

Figure 10. Three arbitrarily assumed pressure distributions used to calculate the minimum temperature distribution needed to maintain saturation if inlet saturated air temperature is 80° F.

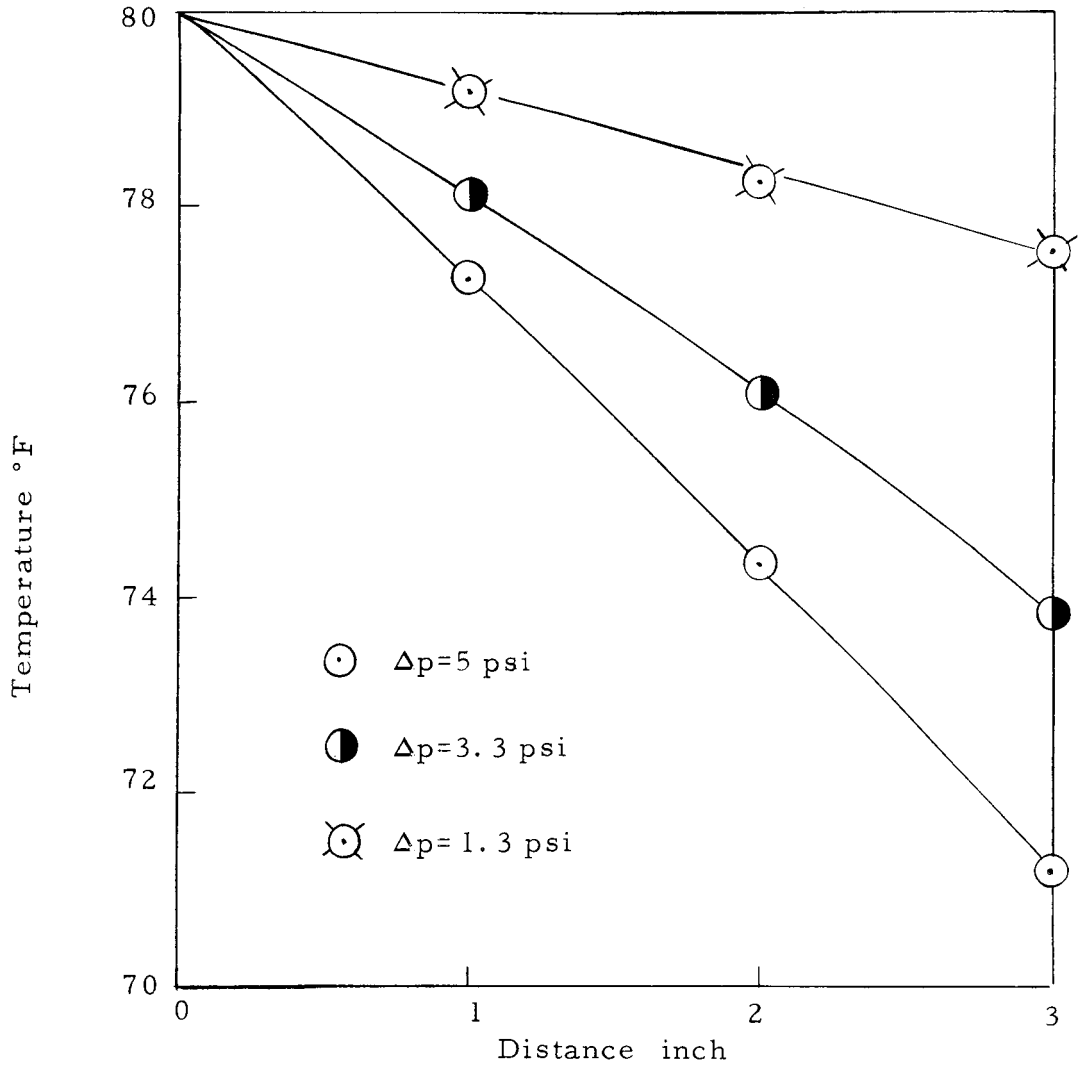

Figure 11. Minimum temperature distribution required to maintain saturation

or

$$\frac{d\omega}{dx} = \frac{(n-1)C_p}{i_{vf}} \frac{dT}{dx} \tag{22}$$

where (n-1) is a constant of proportionality determined by the following expression:

$$n-1 = \frac{i_{vf}(\omega_L - \omega_0)}{C_p(T_L - T_0)} .$$

The symbol, T_L, represents the temperature of the saturated air at exit and ω_L is the corresponding specific humidity. Integrating equation 22 and substituting the value for n will give

$$\omega = \frac{\omega_L - \omega_0}{T_L - T_0} (T - T_0) + \omega_0 . \tag{23}$$

To demonstrate the accuracy of the above approximation, a temperature distribution and a pressure distribution similar to some of those measured later in the experiment are shown by Figure 12. The specific humidity has been calculated by using equation 23 and by the exact method. The exact method consists of three steps:

1. Determining the minimum temperature distribution required to maintain saturated air flow.

2. Using equation 20 to calculate the change of specific humidity in the portion where the temperature of the air-water vapor mixture is lower than the minimum temperature distribution.

3. The specific humidity is constant in the portion where the temperature of the air-water vapor mixture is higher than the minimum temperature distribution.

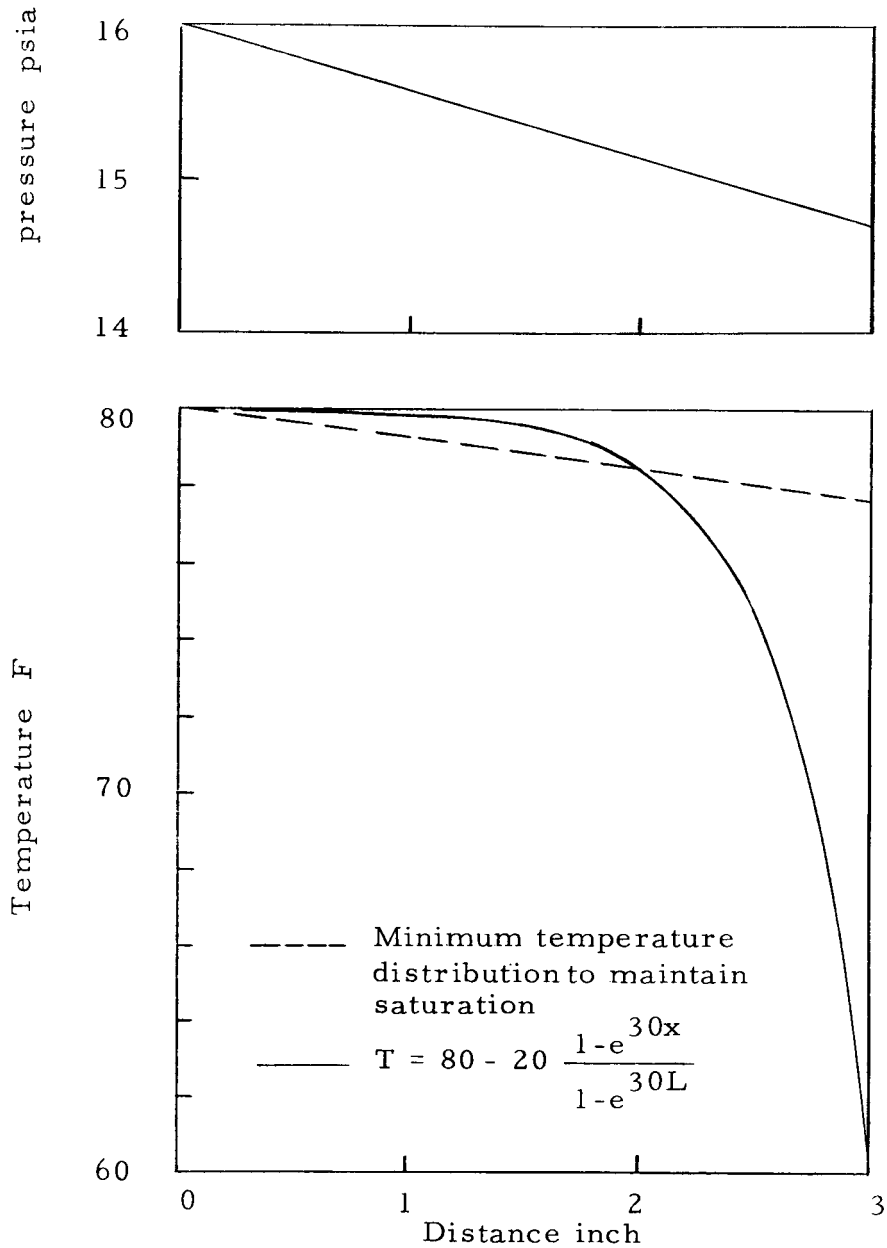

Figure 12. Arbitrarily chosen pressure and temperature distribution to calculate the specific humidity by two different methods.

In Figure 14, the gradient of the specific humidity predicted by equation 22 is compared with the gradient of the exact curve in Figure 13. The gradient in the exact case is obtained by numerical approximation from Figure 13. Notice that the approximation of equation 22 removes the discontinuity of $\frac{d\omega}{dx}$ for this particular case and shows a maximum error at the discontinuity. For the cases where the temperature distribution lies below the minimum temperature distribution throughout the porous bed, there will be no discontinuity in $\frac{d\omega}{dx}$. Hence equation 22 is a reasonable approximation for either of these two possible situations. Using the approximation of equation 22, equation 19 becomes

$$\frac{d^3T}{dx^3} + \frac{\bar{h}S}{nGC_p}\frac{d^2T}{dx^2} - \frac{\bar{h}S}{\bar{K}}\frac{dT}{dx} = 0$$

or

$$\frac{d^3T}{dx^3} + a\frac{d^2T}{dx^2} - b\frac{dT}{dx} = 0$$

where $a = \frac{\bar{h}S}{nGC_p}$, and $b = \frac{\bar{h}S}{\bar{K}}$. The solution to the above differential equation is

$$T = C_1 + C_2 e^{\lambda_2 x} + C_3 e^{\lambda_3 x} \qquad (24)$$

where

$$\lambda_2 = \frac{-a - \sqrt{a^2+4b}}{2}$$

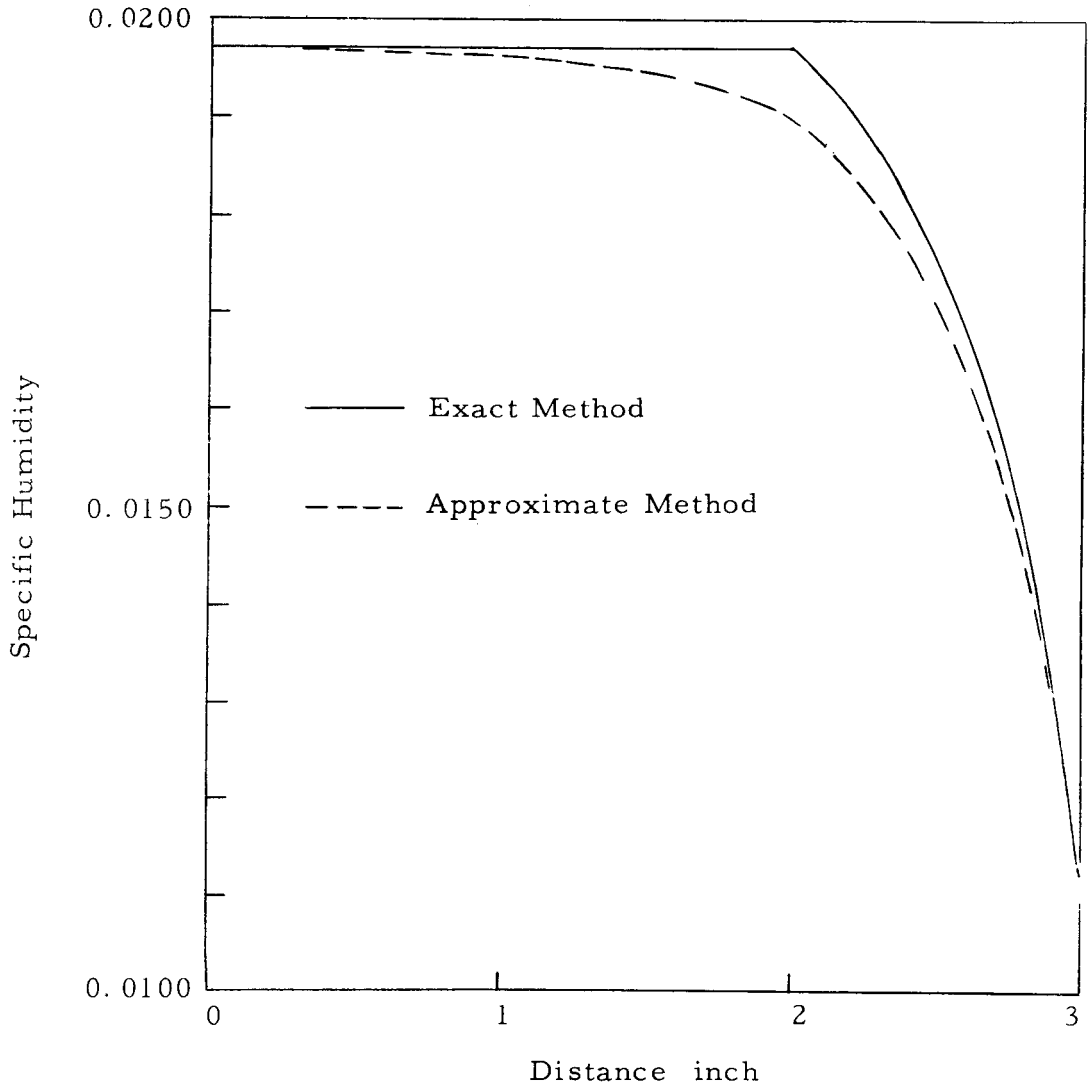

Figure 13. Comparison between two methods in evaluating specific humidity.

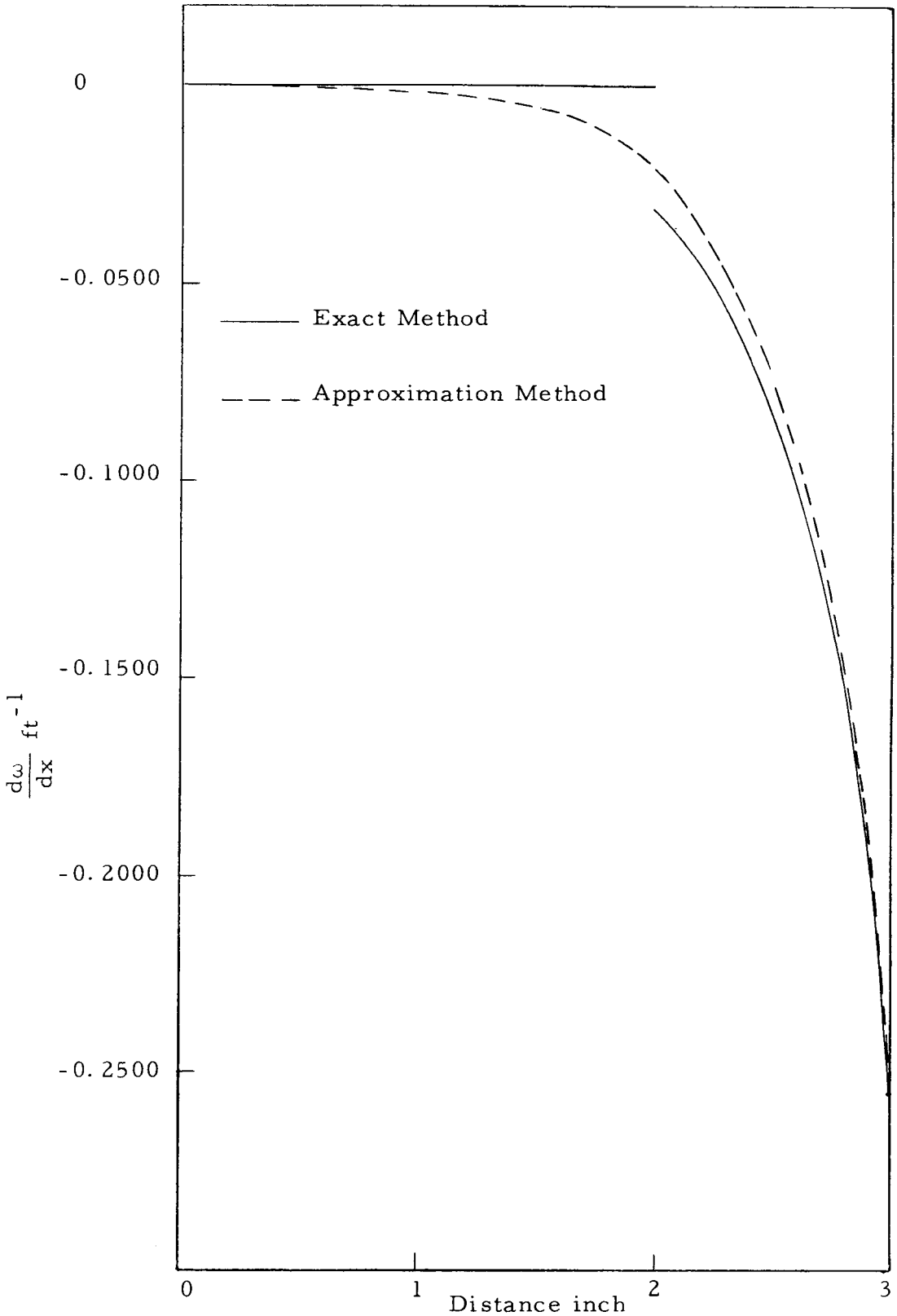

Figure 14. Comparison between exact and approximate way of evaluating the gradient of specific humidity.

and

$$\lambda_3 = \frac{-a + \sqrt{a^2 + 4b}}{2} \quad .$$

Expanding $(a + 4b)^{1/2}$ by Binomial theorem and taking the first two terms gives:

$$\lambda_2 \simeq -a - \frac{b}{a}$$

and

$$\lambda_3 \simeq \frac{b}{a} \quad .$$

By using typical values of a and b, it can be shown that λ_2 is a very large negative number while λ_3 is approximately equal to $\frac{nGC_p}{\bar{K}}$. The error introduced by rounding off higher order terms is generally between 1 to 2%. Evaluation of the integration constants C_1, C_2, and C_3 is discussed in Appendix A where it is found that C_2 is approximately zero. The final result of the air-water vapor temperature distribution is

$$T = T_0 - (T_0 - t_L) \frac{1 - e^{\lambda_3 x}}{1 - e^{\lambda_3 L}} \quad . \qquad (25)$$

Looking at equation 25, it is apparent that the temperature distribution depends upon the value of λ_3 and L. The dimensionless temperature distribution with $\lambda_3 L$ as a parameter is plotted in Figure 15. If the flow rate is high, the thermal conductivity of the porous bed is small, and L is large, there will be only a small

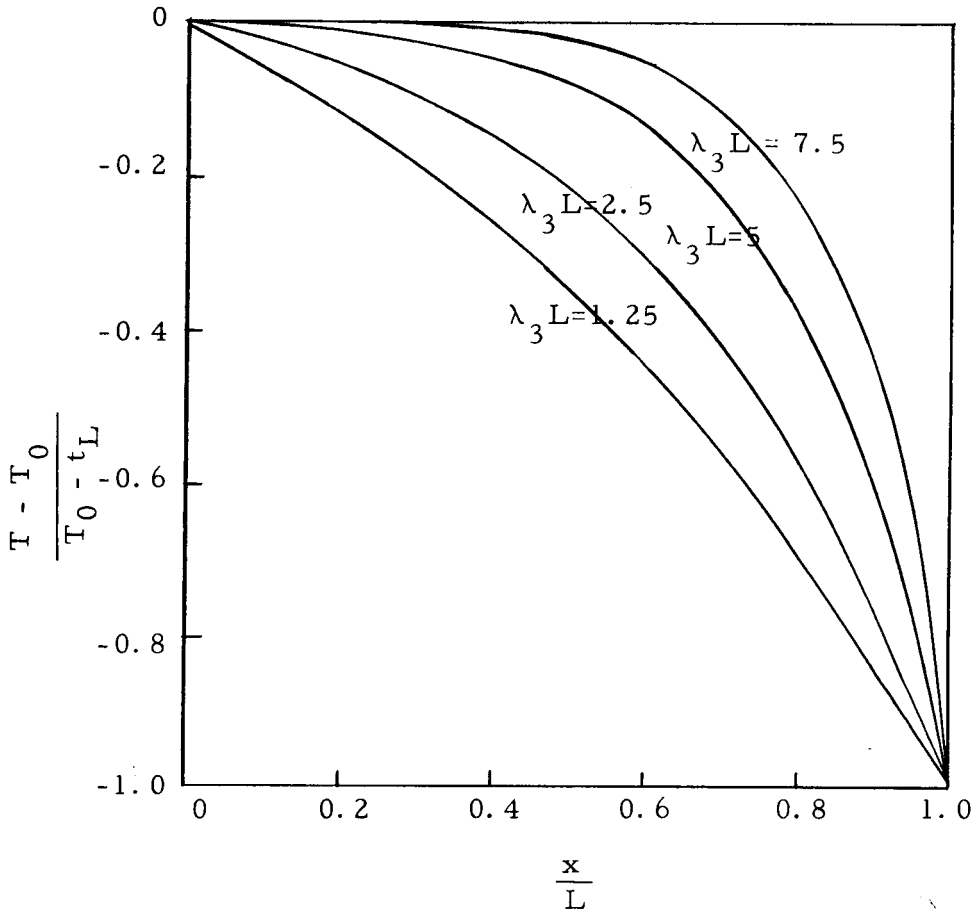

Figure 15. Temperature distribution with $\lambda_3 L$ as a parameter.

temperature drop in the beginning portion of the bed. Contrarily, if the flow rate is low, the thermal conductivity of the bed is large, and L is small, the temperature distribution will be closer to a linear one.

The temperature distribution in the solid particles can be found by substituting the solution 25 and equation 22 into equation 18.

$$t = \frac{GC_p}{\bar{h}S} \frac{T_0 - t_L}{1 - e^{\lambda_3 L}} \lambda_3 e^{\lambda_3 x} + \frac{G(n-1)C_p}{\bar{h}S} \frac{T_0 - t_L}{1 - e^{\lambda_3 L}} \lambda_3 e^{\lambda_3 x} + T.$$

The difference between the solid temperature and the gas temperature can be written as

$$t - T = \frac{\lambda_3}{a} \frac{T_0 - t_L}{1 - e^{\lambda_3 L}} e^{\lambda_3 x} . \qquad (26)$$

Since $\frac{\lambda_3}{a}$ is a very small number and has been assumed to be equal to zero during evaluation of integration constants, the temperature difference between the gas and the solid is equal to zero throughout the thickness of the porous bed according to this assumption. But in reality, there is a small difference between these two temperatures to cause the necessary heat transfer.

The average final percent of moisture content between x_1 and x_2 can be found as follows:

$$\% = \frac{\int_{x_1}^{x_2} \dot{W}_c \, \Theta A \, dx}{\int_{x_1}^{x_2} \rho_s A \, dx}$$

where Θ is the total operation time, and A is the cross section area of the porous bed. By using equation 16 and 22, the above expression becomes

$$\% = \frac{-\frac{\Theta G C_p (n-1)}{i_{vf}} \int_{x_1}^{x_2} \frac{dT}{dx} \, dx}{\rho_s \int_{x_1}^{x_2} dx} .$$

Therefore,

$$\% = \frac{-(n-1) G C_p \Theta (T_2 - T_1)}{i_{vf} \rho_s (x_2 - x_1)} \qquad (27)$$

where T_2 and T_1 correspond to the temperature of moist air at x_2 and x_1.

APPARATUS AND PROCEDURE

Apparatus

The apparatus used in the experiments was the same one built by Mr. John E. Postlewaite (10). The porous column was placed in a plastic tube having an inside diameter of 5.5-inch and an outside diameter of 6-inch. The length of the plastic tube was nine inches, and it had flanges for bolting to the cooling plate and the bubble column (Figure 16). A 150-mesh inconel screen was placed 3-inch from the top of the plastic tube, and the soil was placed on the screen. A similar screen was placed on top of the soil column. A total of fourteen 3/8-inch holes were drilled on the side of the plastic tube to allow the insertion of pressure taps and thermocouples.

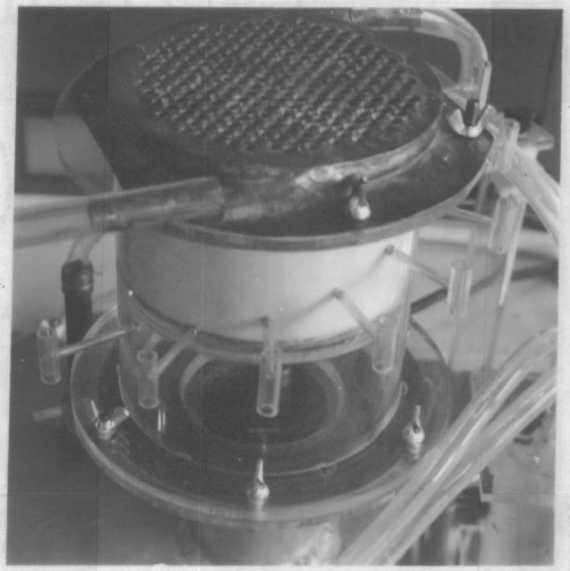

Figure 16. Test section and cooling plate

A heat exchanger was placed on top of the soil column to keep it at a constant temperature. It was made of copper, and had a series of tubes to allow for gas flow through it. The ratio of total hole area to solid area was 0.40 which equalled the average porosity of the soil

or glass beads used in the tests. The cooling water was circulated inside the heat exchanger around the tubes. The cooling water was pumped from a constant temperature water bath at a very high flow rate. There was no detectable temperature gradient in the cooling plate.

Saturated air at a constant temperature was forced through the soil column from the bottom and exhausted at the top at a pressure approximately equal to atmospheric pressure. Saturation of the air was obtained by bubbling it through a 9-inch by 1 1/4-inch diameter porous glass filter at the bottom of a 4-foot column of water. It was assumed that the air-water vapor mixture leaving the top surface of the water column was saturated. The saturation chamber was 1-foot in diameter and 5-feet high. It was made of aluminum and was very well insulated. The air was supplied from a 1/6-hp compressor. For those runs in which condensation was not desired, low humidity room air was passed through a copper coil in the bubble column. The schematic diagram of the whole system is presented in Figure 17.

The temperature of the constant temperature bath and the saturation chamber was controlled to ±0.1°F by two Electron-O-Therm Sr. Temperature controllers (Figure 18). Each temperature

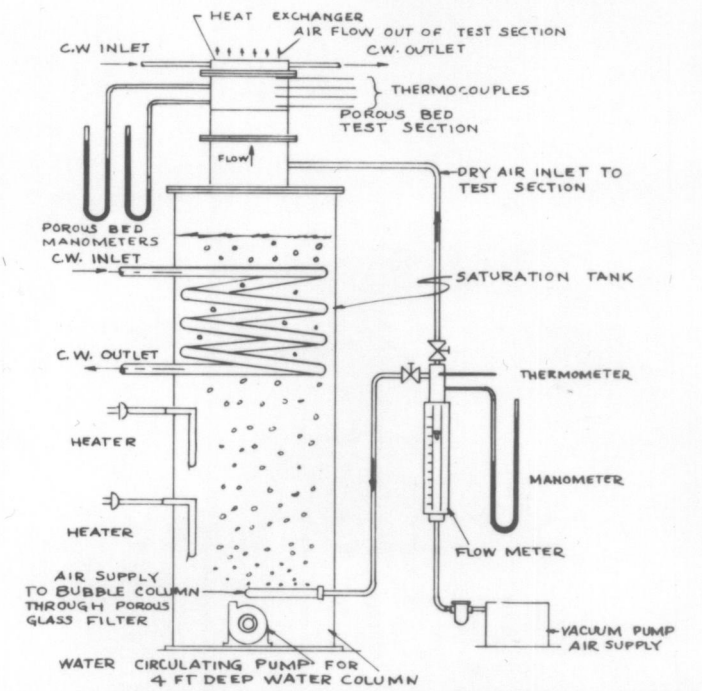

Figure 17. Schematic diagram of the equipment

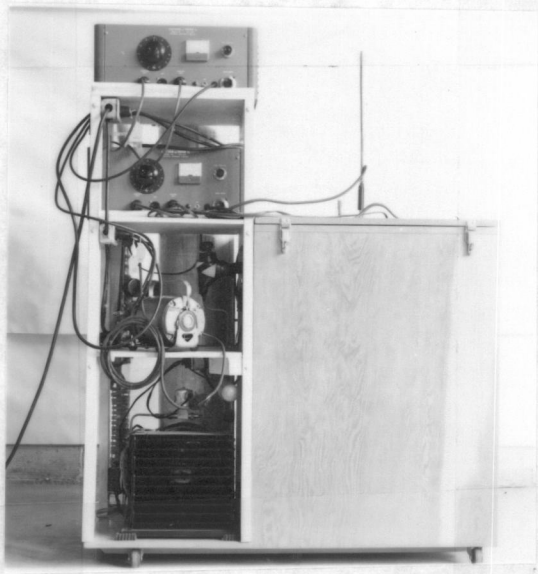

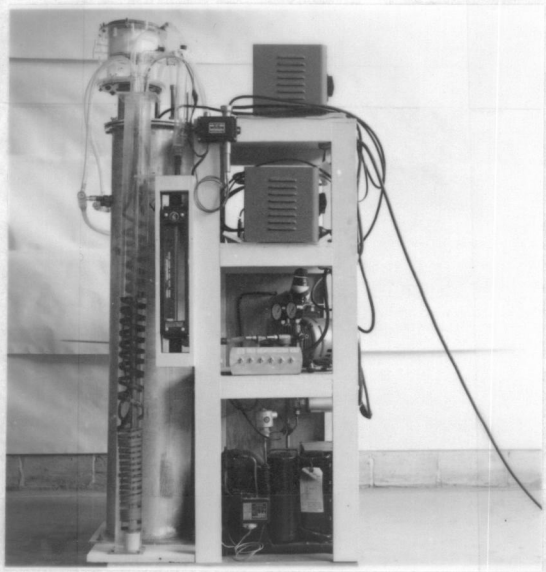

Figure 18. The front and side view of the apparatus

controller consisted of a variac, an electronic circuit, and a resistance thermometer. The variac controlled a 750-watt submersed heater. The electronic circuit controlled a 250-watt submersed heater.

Procedure

The porous material was placed in the test section with great care to insure uniform compaction. Low humidity room air was forced through the porous column to establish the desired initial temperature distribution without causing condensation during the pre-run work. The temperature of low humidity room air was approximately the same as the temperature of the saturated air used later. After the temperature distribution of the dry air reached steady state, the saturated air was turned on.

Temperatures were measured by thermocouples and thermometers at an interval of every 30 minutes. Thermocouples were located in the test section along the flow path with an accuracy of ± 1/32-inches. The uncertainty of the temperature measurement is estimated to be ± 0.5 °F.

Pressure readings were obtained by using manometers. The uncertainty of the measurement was ± 2%. The mass flow rate of dry air was measured with an accuracy of ±4%.

The moisture distribution was determined by taking samples from the porous column at the end of the experiment. The difference between the wet and dry weight divided by the weight of the dry solid particles gave the percentage of moisture content.

The thermal conductivity of quartz sand versus moisture content is plotted in Figure 19. Since there is no information available concerning the variation of thermal conductivity with moisture content of different porous beds, it is assumed that the percentage increase in thermal conductivity of glass beads, sandy soil, and the mixture of glass beads and chrome powder with moisture content is roughly the same as with quartz sand.

In order to estimate the error introduced by rounding off higher order terms when λ_2 and λ_3 were evaluated, the value of film coefficient is needed. The expression given by Hougen and Wilke (8) is as follows:

$$\frac{h}{C_p G} = 1.96 \left(\frac{D_p G}{\mu} \right)^{-0.51} \left(\frac{C_p \mu}{K_f} \right)^{-2/3} .$$

The value of $\bar{h}$ is about 23 BTU/F°-ft^2-hr for coarse glass beads at a typical Reynolds number of 0.35 and is higher for fine glass beads for the same mass flow rate of dry air.

To evaluate λ_3 in equation 24 for different experiments, it is necessary to find $\bar{K}$ which is an average value not only in the sense

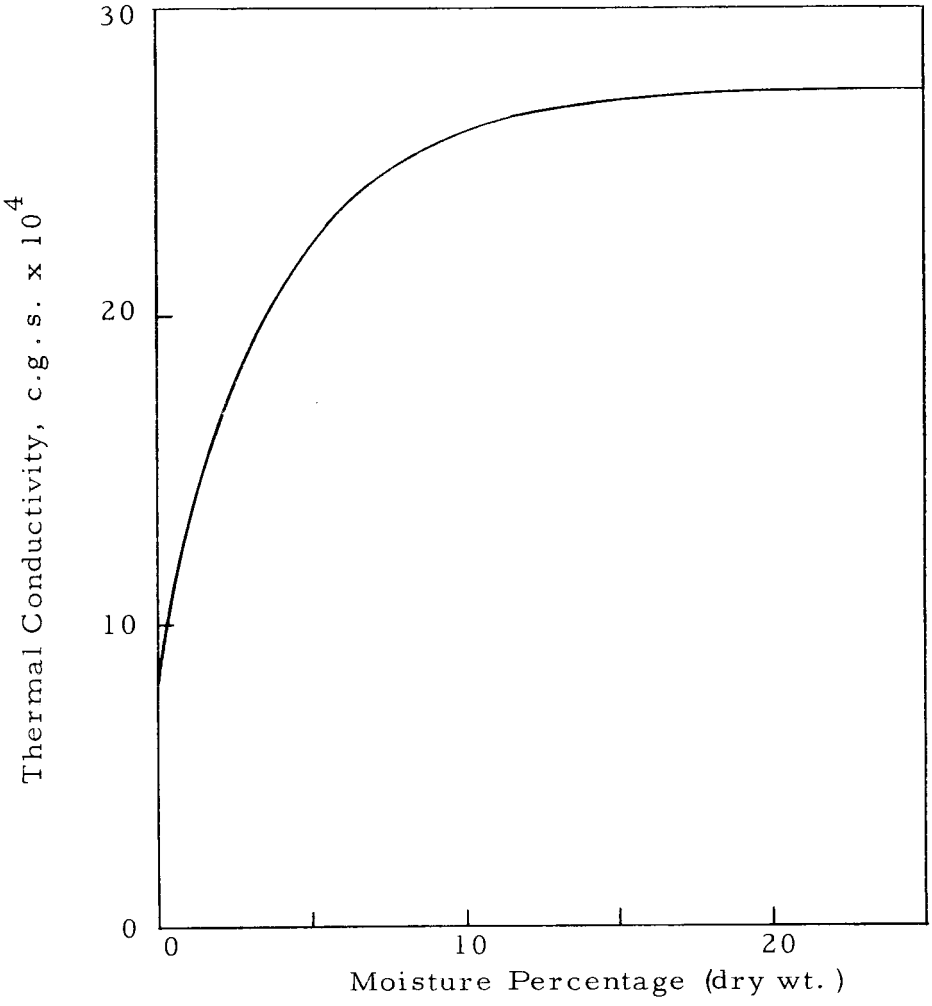

Figure 19. Thermal conductivity of coarse quartz sand (p. 377 Baver's Soil Physics)

of time but also in the sense of space. Since the moisture distribution, in general, is not uniform, the thermal conductivity of a porous bed varies from the drier zones to the wetter zones. This assumption made about $\bar{K}$ causes a large discrepancy between the theoretical prediction and the experimental results. The determination of $\bar{K}$ for each experiment is obtained first by finding the average moisture content using the following equation:

$$\% = \frac{(\omega_L - \omega_0)\, G\, (\frac{\Theta}{2})}{\rho_s L}$$

The average moisture content is then multiplied by $\frac{\rho_s}{\rho_q}$ where ρ_q is the bulk density of quartz sand. Using this new average moisture content and Figure 19, the percentage increase in thermal conductivity can be calculated. With this information and Table 1, the value of $\bar{K}$ can be determined.

RESULTS AND DISCUSSION

Five experiments were performed to verify the theory. Coarse glass beads of 0.011-inches average diameter were used in experiment A and those of a smaller size of 0.001-inches average diameter were used in experiment B. In order to change the thermal conductivity of the porous bed, chrome powder was mixed with fine glass beads. In experiment C, a ratio by weight of 2/3 fine glass beads to 1/3 chrome powder was used as the porous bed. The opposite ratio was used in experiment D. The thermal conductivity of the mixture of chrome powder and fine glass beads was calculated by proportion on a volume basis. Sandy soil was used in experiment E. Some physical properties of these different porous beds are listed below:

Table 1. Physical properties of different porous beds

Porous material	Thermal conductivity BTU/ft-F-hr	Bulk density lb/ft^3	Specific surface ft^2/ft^3
Coarse glass beads	0.16	94	5,400
Fine glass beads	0.117	94	43,000
Chrome powder	0.287	230	-----
1/3 chrome powder 2/3 glass beads	0.15	116	-----
2/3 chrome powder 1/3 glass beads	0.20	151	-----
Sandy soil	0.218	100	-----

A comparison of the predicted and measured temperature distributions of experiments A, B, C, D, and E is plotted in Figure 20. Curve F in Figure 20 is one of the experiments reported by Postlewaite (10). The thermal conductivity of the porous bed was increased to 2.1 BTU/ft-hr-°F by using stainless steel pins. The resulting small value of $\lambda_3 L$ serves as an excellent comparison with the other data. The results in Figure 20 generally follow what has been predicted in Figure 15. The highest value for $\lambda_3 L$ (13.7) was obtained in experiment A by using coarse glass beads which have low thermal conductivity. Therefore, there is no appreciable temperature drop in the beginning 60% of the porous bed. The largest temperature drop occurs in the later portion of the bed. Although the thermal conductivity of fine glass beads is lower than that of coarse glass beads, the value of $\lambda_3 L$ (5.8) for run B is less than in experiment A because the porous bed in experiment B was shortened to 1-inch. The smallest value of $\lambda_3 L$ is 0.30 obtained in experiment F. Hence the temperature distribution is the steepest. The temperature distributions of experiment B, C, D, and E lie between the temperature distribution of experiment A and F in an order predicted in Figure 15. A table which contains the calculation of $\lambda_3 L$ for each experiment is given on page 42.

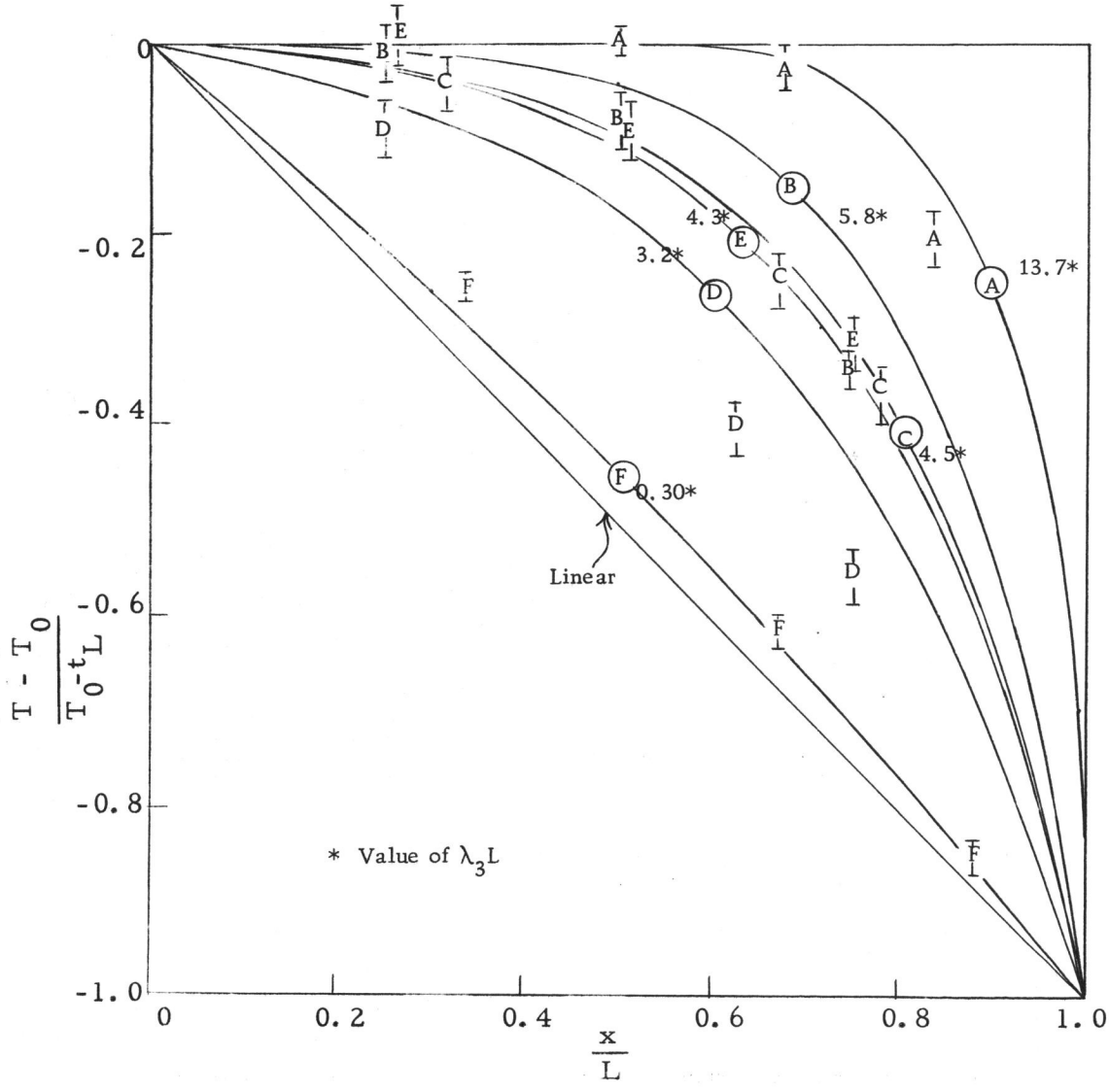

Figure 20. Comparison between predicted and measured temperature distribution.

Table 2. Calculation of $\lambda_3 L$ for each experiment

Exp.	$\omega_0 - \omega_L$	$T_0 - t_L$	n	Average Moisture Content	G	$\bar{K}$	λ_3	$\lambda_3 L$
A	0.0089	17.2	3.27	2%	21.2	0.304	55	13.7
B	0.0070	15.7	2.9	2%	23	0.228	69.5	5.8
C	0.0066	17	2.71	1.9%	23.9	0.29	53.5	4.5
D	0.0070	17.5	2.74	2%	23.3	0.40	38.4	3.2
E	0.0079	18	3.3	1.8%	23	0.35	52	4.3
F	0.0055	13.1	2.84	1.8%	8.1	2.2	2.4	0.30

The discrepancy between the experimental results and the theoretical prediction for experiment B may be caused by heavy moisture deposits in the portion of the bed near the cooling plate which causes a large increase in thermal conductivity. Consequently, the temperature drops excessively in that portion of the bed. The discrepancy in experiment D may be caused by the inaccuracy in calculation of $\bar{K}$.

The pressure distribution has been calculated by substituting the temperature distribution into equation 15 which yields

$$P_a^2 = C_2 \left\{ \left(T_0 - \frac{T_0 - t_L}{1 - e^{\lambda_3 L}}\right) x + \frac{(T_0 - t_L)\, e^{\lambda_3 x}}{\lambda_3 (1 - e^{\lambda_3 L})} \right\} + C_3$$

where

$$C_2 = \frac{P_0^2 - P_L^2}{\left(T_0 - \frac{T_0 - t_L}{1 - e^{\lambda_3 L}}\right) L + \frac{(T_0 - t_L)\,(e^{\lambda_3 L} - 1)}{(1 - e^{\lambda_3 L})\lambda_3}}$$

$$C_3 = P_0^2 - \left(\frac{T_0 - t_L}{1 - e^{\lambda_3 L}}\right) \frac{1}{\lambda_3} \left[\frac{P_0^2 - P_L^2}{\left(T_0 - \frac{T_0 - t_L}{1 - e^{\lambda_3 L}}\right) L + \frac{(T_0 - t_L)(e^{\lambda_3 L} - 1)}{(1 - e^{\lambda_3 L})\lambda_3}} \right].$$

The results for coarse and fine glass beads are presented in Figures 21 and 22. The deviation of measured pressure from predicted pressure at any location along the porous bed is believed to be caused by uneven compaction. Data on pressure distribution for the other three tests are given in Appendix B.

The calculated and measured moisture distribution for experiments A, B, C, D, E, and F are compared in Figures 23, 24, 25, 26, 27, and 28. The predicted moisture distribution is obtained by using equation 27. Six samples were taken for each layer and the cross-sectional variation of moisture content is less than ± 10% of the average value. This variation may be caused again by uneven compaction, radial temperature gradient, or the technique of sampling. Only average moisture content of each layer is plotted against distance in above figures. It is interesting to note here that the moisture distribution in the porous bed becomes more uniform as the value of the parameter, $\lambda_3 L$, decreases. When $\lambda_3 L$ equals 0.30, the moisture distribution becomes very close to uniform (Figure 28).

The mathematical treatment of this problem has served as a guide to understand the physical phenomenon. The quantitative agreement between theory and experiment can be further improved

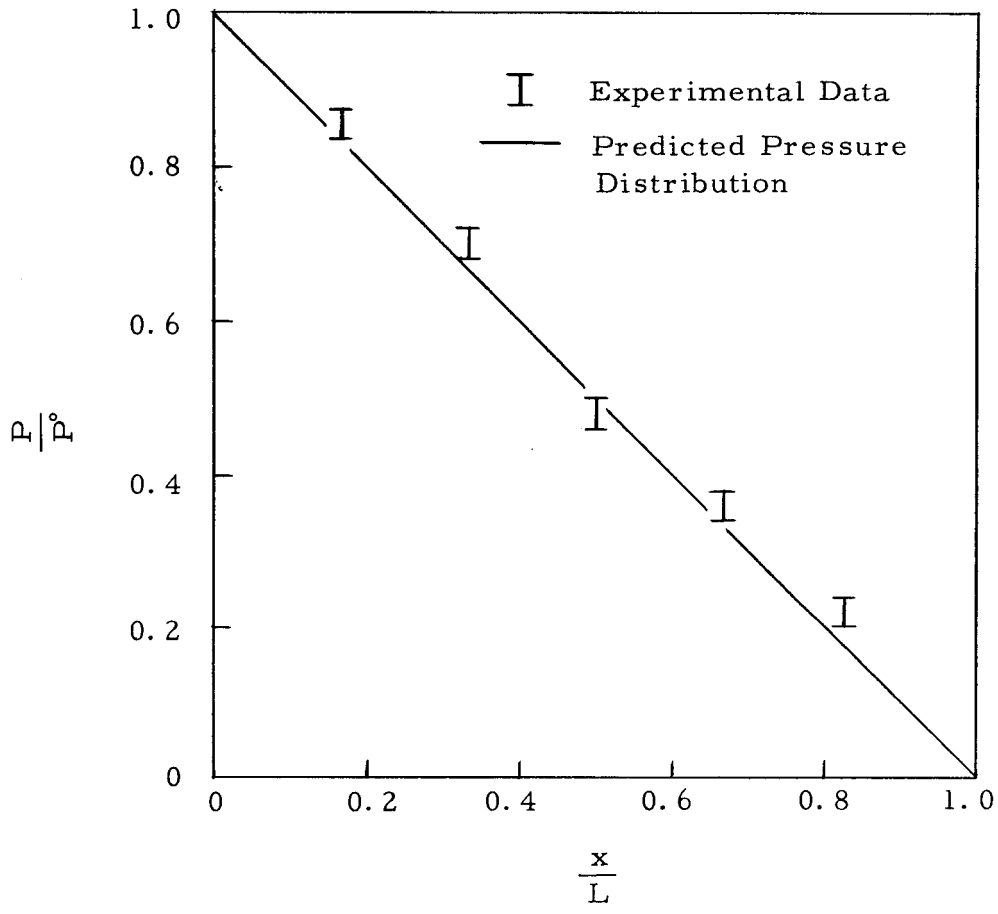

Figure 21. Pressure distribution in a 3" long coarse glass beads column

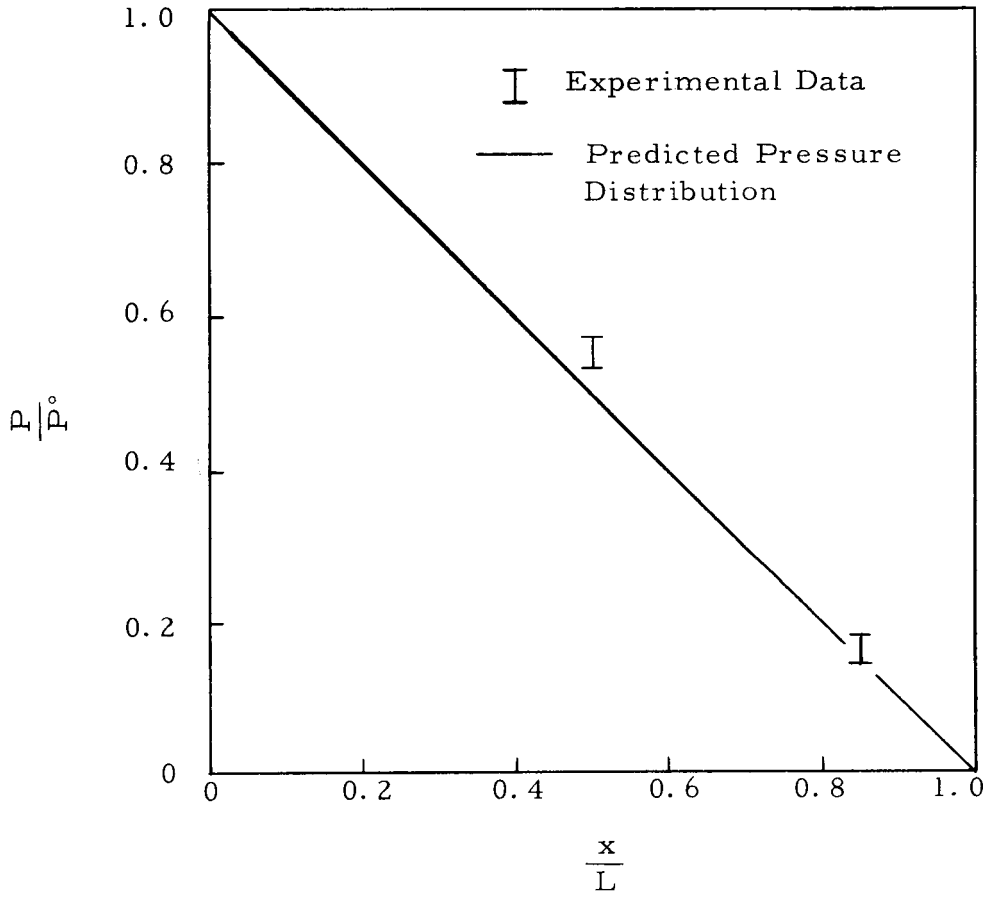

Figure 22. Pressure distribution in a 1" long fine glass beads column

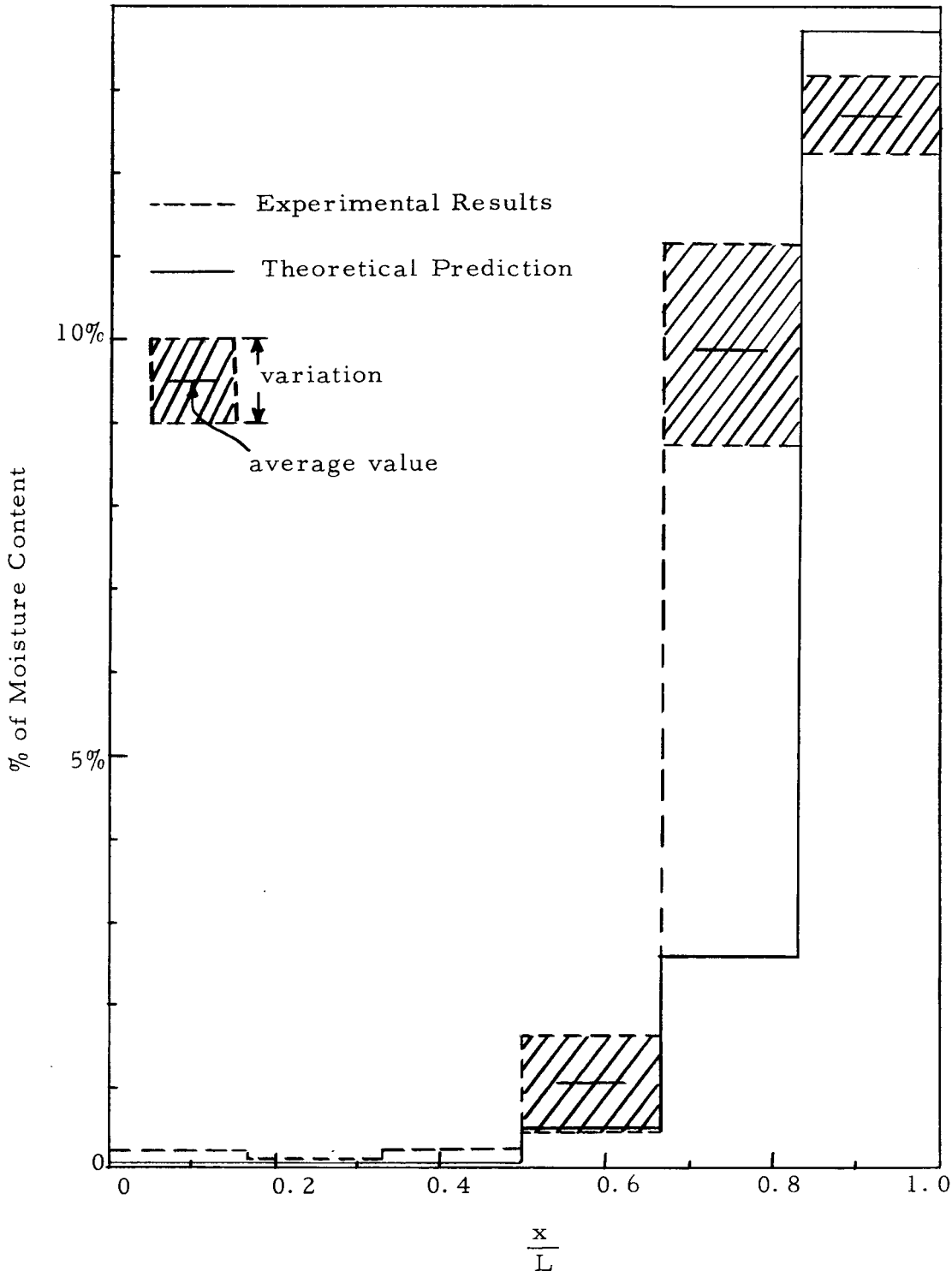

Figure 23. Moisture distribution in coarse glass beads ($\lambda_3 L=13.7$).

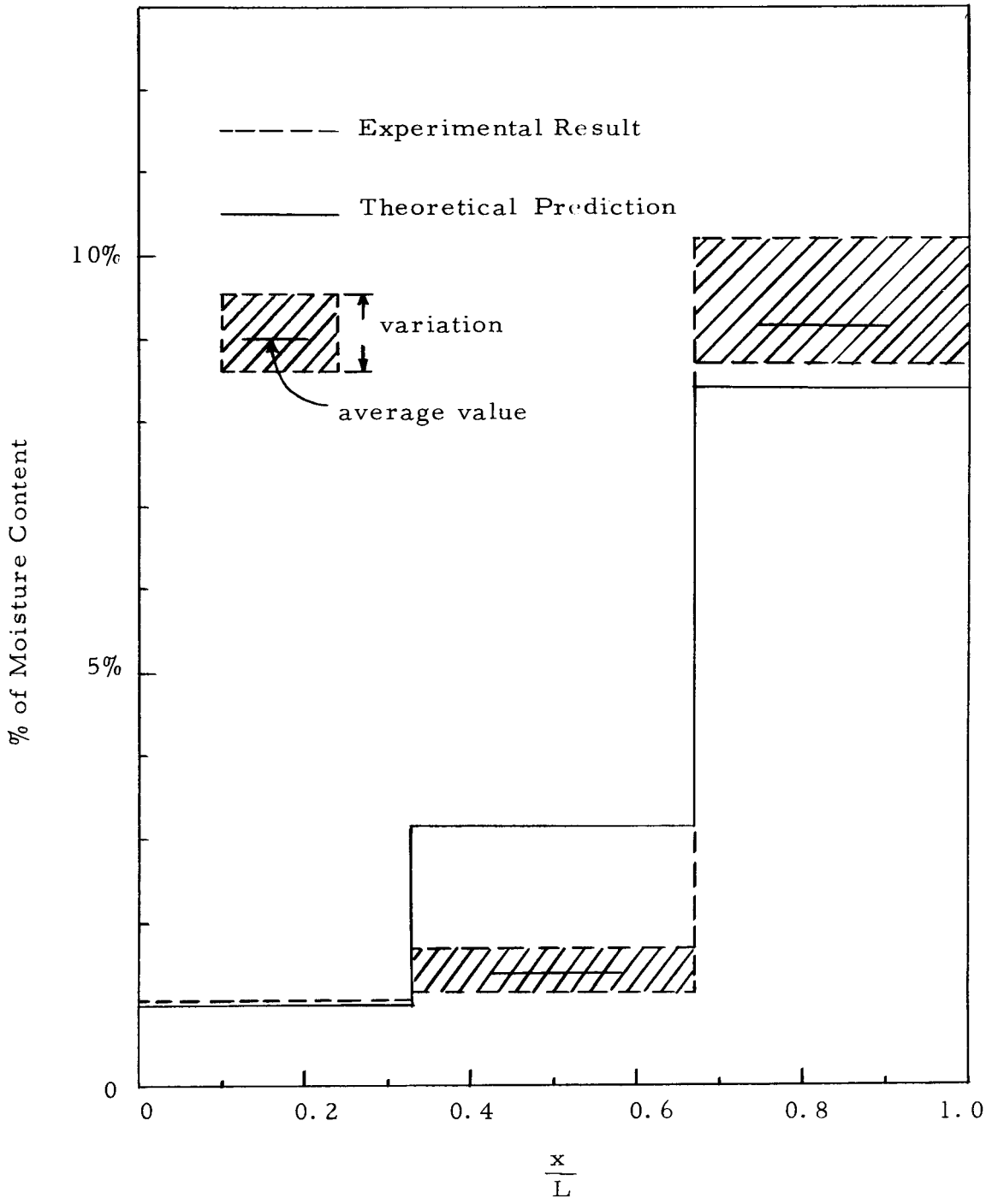

Figure 24. Moisture distribution in fine glass beads ($\lambda_3 L = 5.8$)

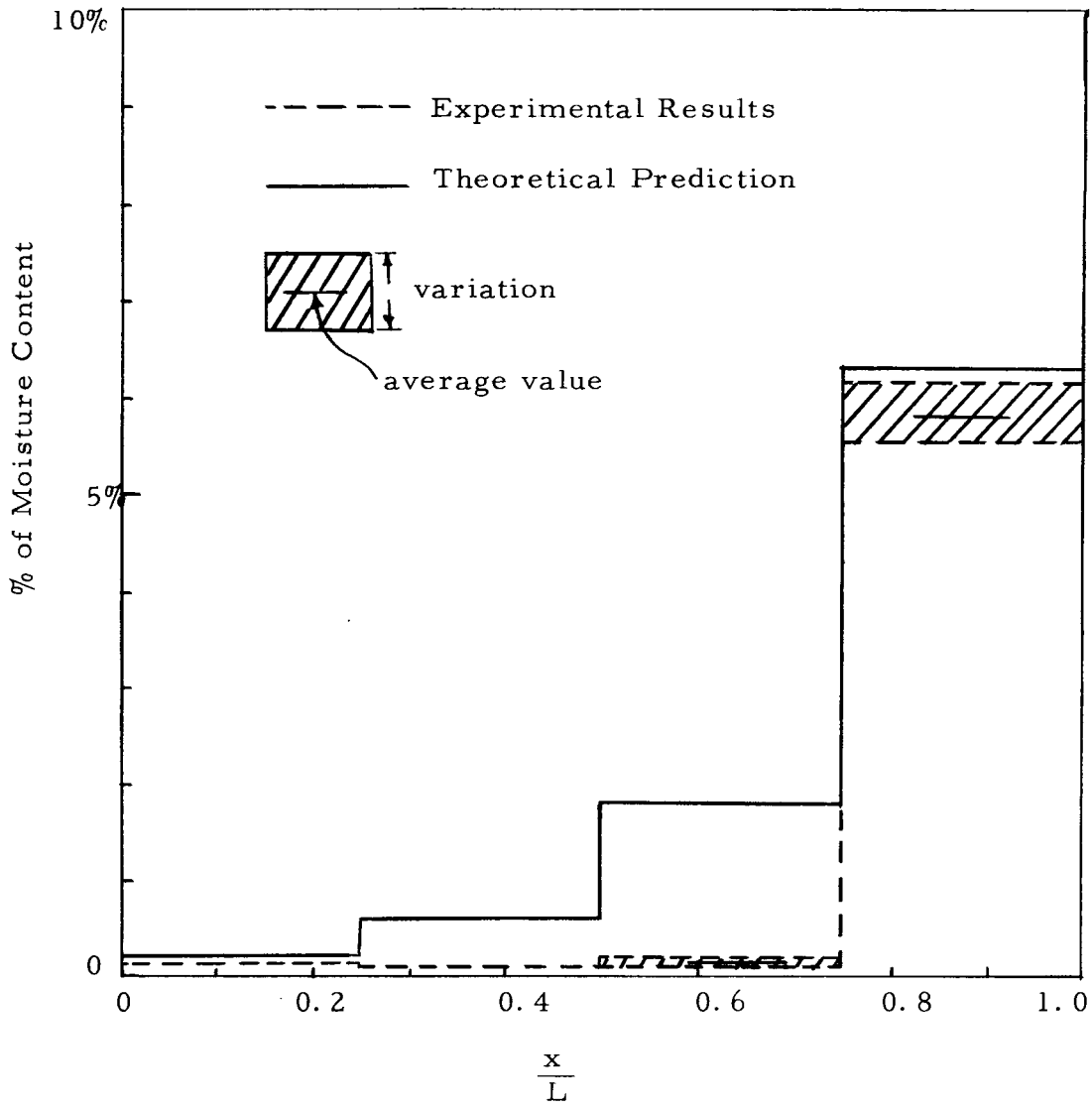

Figure 25. Moisture distribution in fine glass beads and chrome powder mixture (2/3 fine glass beads, 1/3 chrome powder, $\lambda_3 L = 4.5$).

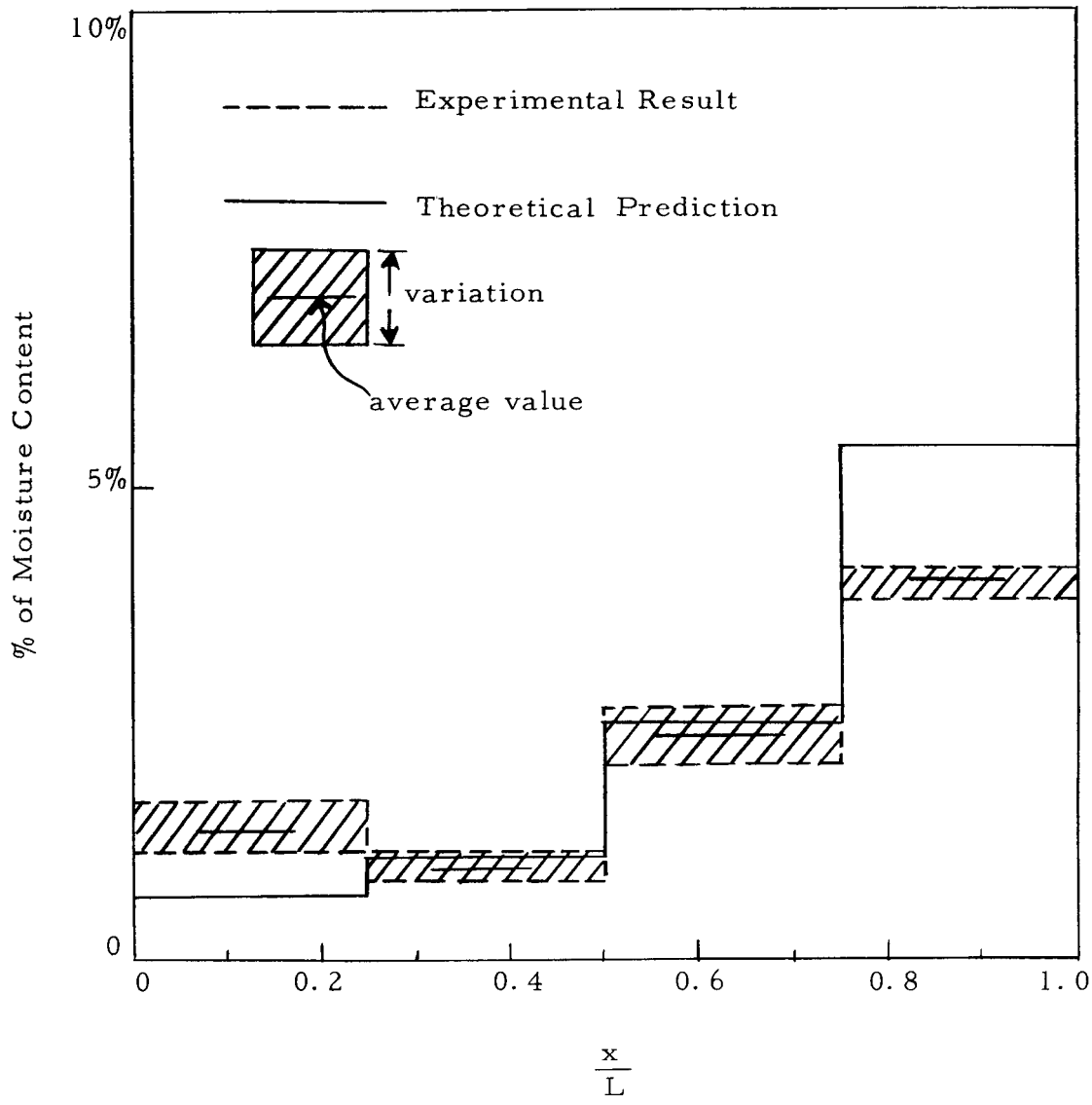

Figure 26. Moisture distribution in fine glass beads and chrome powder mixture (1/3 fine glass beads, 2/3 chrome powder, $\lambda_3 L = 3.2$).

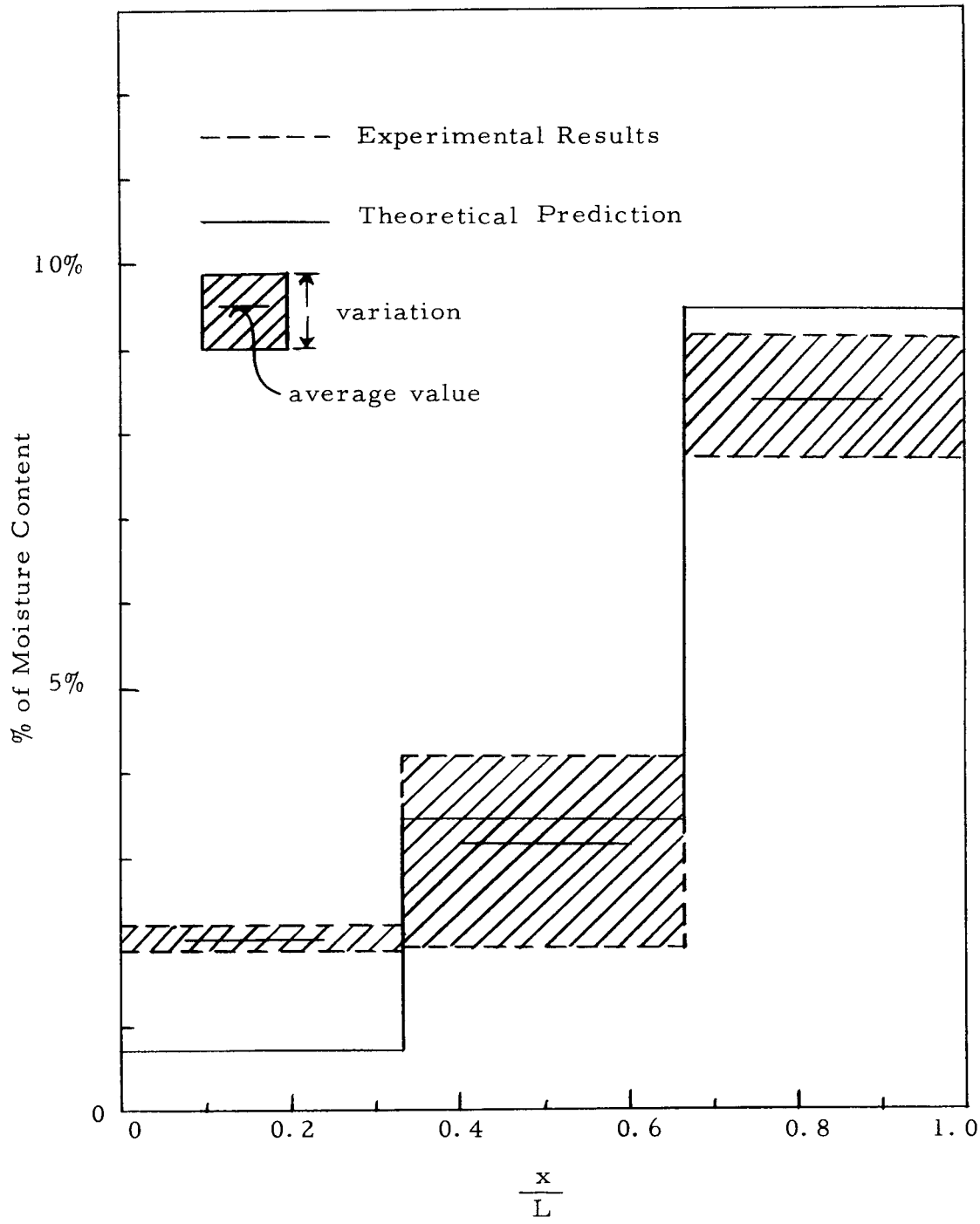

Figure 27. Moisture distribution in sandy soil ($\Lambda_3 L = 4.3$).

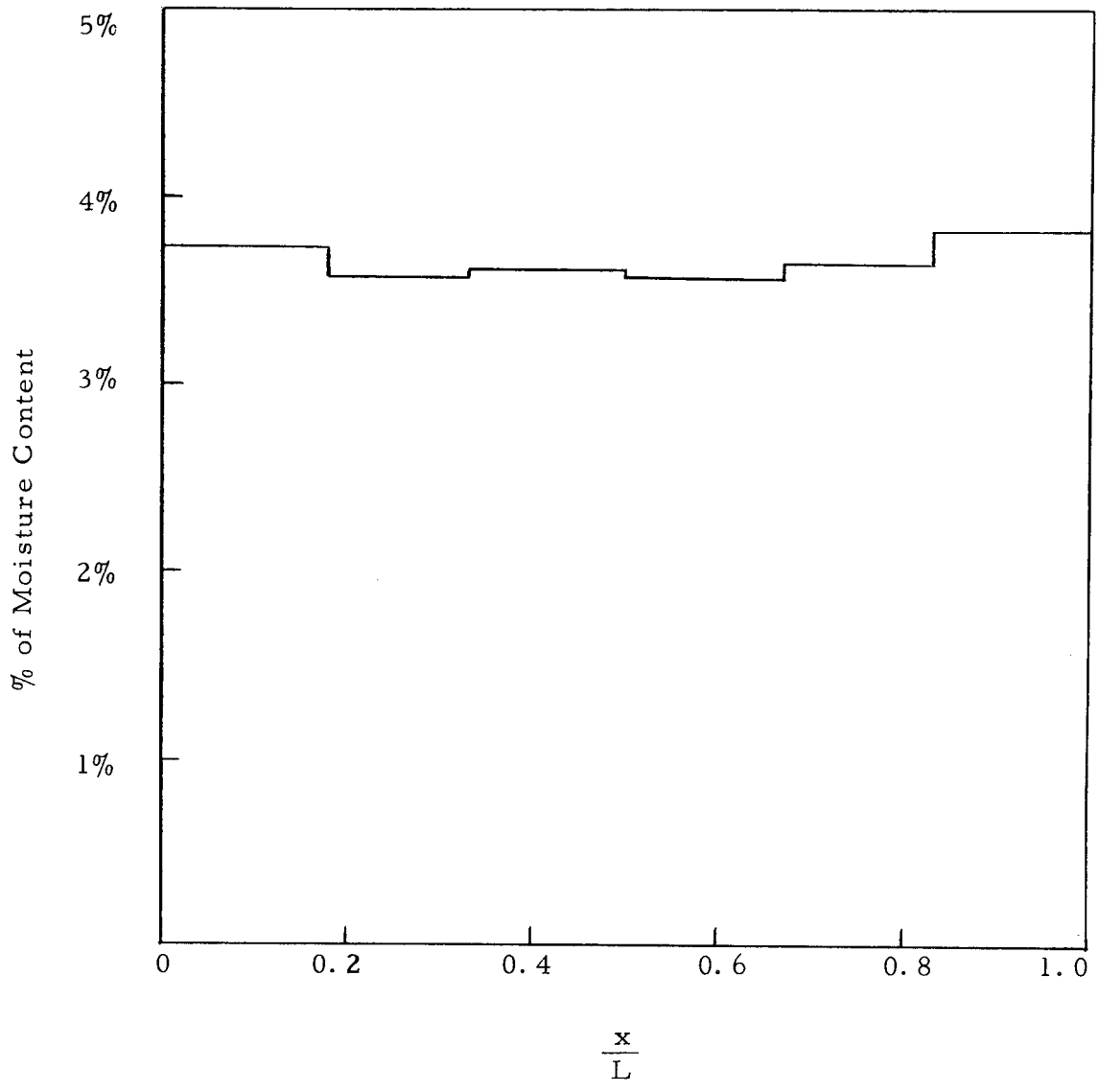

Figure 28. Moisture distribution in sandy soil with stainless steel pins ($\lambda_3 L = 0.30$).

if exact information about the relationship between thermal conductivity and moisture content for the various porous beds is known, and also if a method of obtaining uniform compaction is available. Error caused by neglecting possible variation of $\bar{K}$ with space is not a serious one as far as a study of conditions required for spacewise uniform condensation is concerned. In that case, $\bar{K}$ will be a constant with respect to space.

CONCLUSIONS

It has been shown by the analysis that the parameter, $\frac{nGC_p}{\bar{K}} L$, has the most effect upon the shape of the temperature distribution. The pressure distribution in the porous bed is nearly linear and depends only slightly on the temperature distribution. Both calculated and experimental results show that the moisture distribution becomes uniform when the value of $\frac{nGC_p}{\bar{K}} L$ is equal to 0.30.

The compaction of the porous bed has the most influence on the pressure distribution. The discrepancy between predicted and measured temperature distributions is caused by inaccuracies in evaluating the value of $\bar{K}$. The difficulty of consistent sampling also causes some error in the measured moisture distribution.

In spite of the assumptions which have been made and the uncertainties of physical constants, the analysis agrees with the experimental results within 10 to 20%.

BIBLIOGRAPHY

1. Baver, Leonard D. Soil physics. 3d ed. New York, Wiley, 1956. 370 p.

2. Keenan, Joseph H. and F. G. Keyes. Thermodynamic properties of steam. New York, Wiley, 1936. 89 p.

3. Muskat, Morris. The flow of homogeneous fluids through porous media. Ann Arbor, Michigan, J. W. Edwards, 1946. 755 p.

4. McAdams, William H. Heat transmission. 3d ed. New York, mcGraw-Hill, 1954. 532 p.

5. Schneider, P. J. Conduction heat transfer. Cambridge, Mass. Addison-Wesley, 1955. 395 p.

6. Scheidergger, Adrian E. The physics of flow through porous media. New York, Macmillan, 1960. 308 p.

7. Weinbaum, S. and Wheller, H. L. Jr. Heat transfer in sweat-cooled metals. Journal of Applied Physics 20: 1: 113-122. 1949.

8. Wilke, C. R. and Hougen, O. A. Heat, mass and momentum transfer. Transactions of the American Institute of Chemical Engineers 39: 1-36. 1943.

9. Wolfe, John W. The development of a method for the condensation of moisture uniformly in soil without exceeding field capacity. Ph. D. thesis. Logan, Utah State University, 1959. 57 numb. leaves.

10. Postlewaite, John E. Production of uniform condensation from saturated air flow in cooled porous media. Master's thesis. Corvallis, Oregon State University, 1962.

APPENDIX

APPENDIX A - EVALUATION OF INTEGRATION CONSTANTS

To determine the integration constants in general solution 24. the following boundary conditions are needed:

a. $x = 0 \quad T = T_0$

b. $x = L \quad T = t_L$

c. $x = L \quad -\bar{K}A \frac{dt}{dx} = q$

where q is the amount of heat flow into the cooling plate by conduction and A is the total cross section area of porous column.

Figure 29. Possible heat transfer to cooling plate.

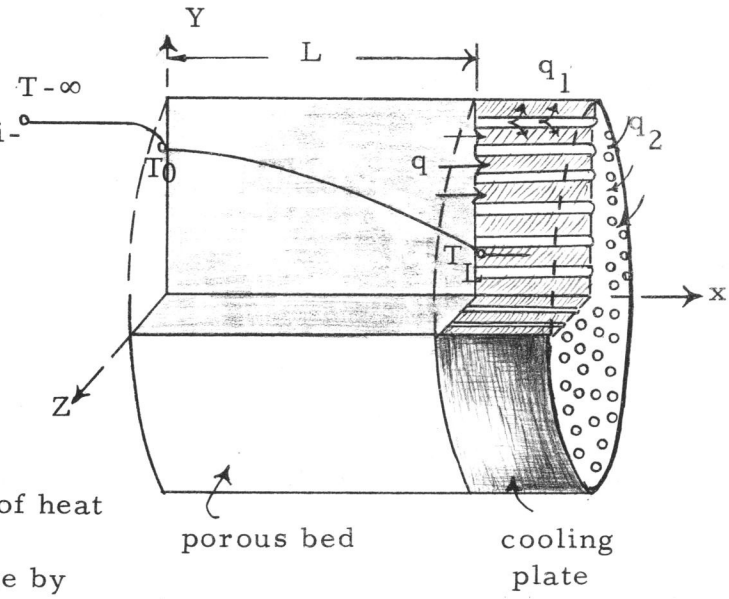

Substituting the above conditions to the solution 24 gives

d. $C_1 + C_2 + C_3 = T_0$

e. $C_1 + C_2 e^{\lambda_2 L} + C_3 e^{\lambda_3 L} + \frac{GC_p n}{\bar{h}S}(C_2\lambda_2 e^{\lambda_2 L} + C_3\lambda_3 e^{\lambda_3 L}) = t_L$

f. $-\bar{K}A[C_2\lambda_2 e^{\lambda_2 L} + C_3\lambda_3 e^{\lambda_3 L} + \frac{GC_p n}{\bar{h}S}(C_2\lambda_2^2 e^{\lambda_2 L} + C_3\lambda_3^2 e^{\lambda_3 L})] = q.$

Since λ_2 is a very large negative number the above equations can be simplified by neglecting the terms involving $e^{\lambda_2 L}$. Writing the equations with this assumption will give

g. $C_1 + C_2 + C_3 = T_0$

h. $C_1 + (e^{\lambda_3 L} + \frac{\lambda_3 e^{\lambda_3 L}}{a}) C_3 = t_L$

$$i.\quad C_3 = \frac{-q}{\bar{K}A\lambda_3 e^{\lambda_3 L}(1+\frac{\lambda_3}{a})} \quad .$$

where $a = \frac{\bar{h}S}{GC_{pn}}$. Hence

$$C_1 = t_L + \frac{q}{\bar{K}A\lambda_3}$$

$$C_2 = T_0 - t_L + \frac{q}{\bar{K}A\lambda_3}\left[\frac{1}{e^{\lambda_3 L}(1+\frac{\lambda_3}{a})} - 1\right]$$

and

$$T = t_L + \frac{q}{\bar{K}A\lambda_3} + \left\{T_0 - t_L + \frac{q}{\bar{K}A\lambda_3}\left[\frac{1}{e^{\lambda_3 L}(1+\frac{\lambda_3}{a})} - 1\right]\right\}$$

$$e^{\lambda_2 x} - \frac{q}{\bar{K}A\lambda_3 e^{\lambda_3 L}(1+\frac{\lambda_3}{a})} e^{\lambda_3 x} \quad .$$

Let $x = L$, then

$$T_L = t_L + \frac{q}{\bar{K}A\lambda_3}\left[1 - \frac{a}{a+\lambda_3}\right] .$$

From the above equation, it is clear that the difference between T_L t_L is

$$\frac{q}{\bar{K}A\lambda_3}\left[1 - \frac{a}{a+\lambda_3}\right] .$$

If the magnitude of the above expression is small, then T_L will be approximately equal to t_L. The value of q can be obtained by two different methods. One is to try to measure it in the laboratory. But due to the very small temperature difference of inlet and outlet

water to the cooling plate, and also other possible heat transfer to the cooling plate, the evaluation of q in this manner is very difficult (Figure 29). Since it is the desire to show that T_L is approximately equal to t_L, the magnitude of q will be estimated as following:

Multiplying equation 10 by dx and integrating between 0 and L gives

$$\int_0^L \bar{K} \frac{d^2t}{dx^2}\, dx + \int_0^L \bar{h}S(T-t)dx = 0$$

or

$$\bar{K} \left.\frac{dt}{dx}\right|_{x=L} - \bar{K} \left.\frac{dt}{dx}\right|_{x=0} + \int_0^L \bar{h}S\,(T-t)dx = 0 .$$

But

$$q = -\bar{K}A \left.\frac{dt}{dx}\right|_{x=L} .$$

Therefore,

$$q = -\bar{K}A \left.\frac{dt}{dx}\right|_{x=0} + A\int_0^L \bar{h}S(T-t)\, dx .$$

From equation 17

$$\bar{h}S(T-t) = -GC_p \frac{dT}{dx} - Gi_{vf} \frac{d\omega}{dx} .$$

Hence,

$$q = -A\left\{\bar{K} \left.\frac{dt}{dx}\right|_{x=0} + GC_p \int_0^L \frac{dT}{dx}\, dx + Gi_{vf} \int_0^L \frac{d\omega}{dx}\, dx \right\} .$$

Since T_0 is always less than or equal to $T_{-\infty}$ and T_L is always

greater than or equal to t_L, q can be expressed by the following inequality

$$q \leqslant -A \{\bar{K} \frac{dt}{dx} \Big|_{x=0} + GC_p \int_{T_{-\infty}}^{t_L} dT + Gi_{vf} \int_{\omega_0}^{\omega_L} d\omega \}$$

where ω_0 and ω_L are evaluated according to the end temperature which is assumed to be $T_{-\infty}$ and t_L. The first term, $\bar{K} \frac{dt}{dx} \Big|_{x=0}$, is always less than $K \frac{t_L - T_{-\infty}}{L}$. Therefore,

$$q \leqslant -A \{\bar{K} \frac{t_L - T_{-\infty}}{L} + GC_p (t_L - T_{-\infty}) + Gi_{vf} (\omega_L - \omega_0) \}$$

If maximum $|t_L - T_{-\infty}| \leqslant 20°F$ and maximum $|\omega_L - \omega_0| \leqslant 0.0106$ which are the upper limit of this problem, then q is equal or less than 352 BTU/hr. Consequently,

$$\frac{q}{\bar{K} A \lambda_3} [\, 1 - \frac{a}{a + \lambda_3} \,] \leqslant 0.4° F$$

or

$$T_L - t_L \leqslant 0.4° F$$

As an approximation, the third boundary condition will be changed to $T = t_L$ at $x = L$. With this modification and also boundary condition a. and b., the integration constants can be evaluated by solving the following equations:

$$\text{j.} \quad C_1 + C_2 + C_3 = T_0$$

$$\text{k.} \quad C_1 + e^{\lambda_2 L} C_2 + e^{\lambda_3 L} C_3 = t_L$$

$$l.\quad C_1 + (1 + \frac{\lambda_2}{a})\, e^{\lambda_2 L} C_2 + (1 + \frac{\lambda_3}{a}) e^{\lambda_3 L} C_3 = t_L$$

The roots of equation j, k, and l are:

$$C_1 = \frac{\begin{vmatrix} T_0 & 1 & 1 \\ t_L & e^{\lambda_2 L} & e^{\lambda_3 L} \\ t_L & (1+\frac{\lambda_2}{a}) e^{\lambda_2 L} & (1+\frac{\lambda_3}{a})\, e^{\lambda_3 L} \end{vmatrix}}{\Delta}$$

$$C_2 = \frac{\begin{vmatrix} 1 & T_0 & 1 \\ 1 & t_L & e^{\lambda_3 L} \\ 1 & t_L & (1+\frac{\lambda_3}{a}) e^{\lambda_3 L} \end{vmatrix}}{\Delta}$$

$$C_3 = \frac{\begin{vmatrix} 1 & 1 & T_0 \\ 1 & e^{\lambda_2 L} & t_L \\ 1 & (1+\frac{\lambda_2}{a}) e^{\lambda_2 L} & t_L \end{vmatrix}}{\Delta}$$

where

$$\Delta = \begin{vmatrix} 1 & 1 & 1 \\ 1 & e^{\lambda_2 L} & e^{\lambda_3 L} \\ 1 & (1+\frac{\lambda_2}{a})e^{\lambda_2 L} & (1+\frac{\lambda_3}{a})e^{\lambda_3 L} \end{vmatrix} .$$

Expanding the determinants will give

$$C_1 = \frac{[\frac{\lambda_3}{a}e^{(\lambda_2+\lambda_3)L} - \frac{\lambda_2}{a}e^{(\lambda_2+\lambda_3)L}]T_0 + [\frac{\lambda_2}{a}e^{\lambda_2 L} - \frac{\lambda_3}{a}e^{\lambda_3 L}]t_L}{\frac{\lambda_3}{a}[e^{(\lambda_1+\lambda_2)L} - e^{\lambda_3 L}] + \frac{\lambda_2}{a}e^{\lambda_2 L}(1 - e^{\lambda_3 L})}$$

$$C_2 = \frac{\frac{\lambda_3}{a}e^{\lambda_3 L}(t_L - T_0)}{\frac{\lambda_3}{a}[e^{(\lambda_1+\lambda_2)L} - e^{\lambda_3 L}] + \frac{\lambda_2}{a}e^{\lambda_2 L}(1 - e^{\lambda_3 L})}$$

and

$$C_3 = \frac{T_0\frac{\lambda_2}{a}e^{\lambda_2 L} - t_L\frac{\lambda_2}{a}e^{\lambda_2 L}}{\frac{\lambda_3}{a}[e^{(\lambda_1+\lambda_2)L} - e^{\lambda_3 L}] + \frac{\lambda_2}{a}e^{\lambda_2 L}(1 - e^{\lambda_3 L})} .$$

Since $\frac{\lambda_3}{a}$ is a very small number, it is reasonable to consider the limiting case when $\frac{\lambda_3}{a}$ becomes zero. Taking limits on C_1, C_2, and C_3 to let $\frac{\lambda_3}{a}$ approach to zero gives

$$\lim_{\frac{\lambda_3}{a} \to 0} C_1 = \frac{t_L - e^{\lambda_3 L}T_0}{1 - e^{\lambda_3 L}}$$

$$\lim_{\frac{\lambda_3}{a} \to 0} C_2 = 0$$

and

$$\lim_{\frac{\lambda_3}{a} \to 0} C_3 = \frac{T_0 - t_L}{1 - e^{\lambda_3 L}} .$$

Hence, the particular solution will be

$$T = T_0 - (T_0 - t_L) \frac{1 - e^{\lambda_3 x}}{1 - e^{\lambda_3 L}}$$

where T_0 and t_L can be easily measured.

APPENDIX B

Experiment A

Porous material: Coarse glass beads

Bulk density, ρ_s: 94 lb/ft^3

Length of porous column, L: 3 inches

Mass flow rate of dry air, G : 21.2 lb/ft^2-hr

Thermal conductivity of the dry porous bed, K: 0.16 BTU/ft-F-hr

Temperature of inlet saturated air, T_0 : 80.3°F

Temperature of solid particles at x = L, t_L : 63.1°F

Pressure of inlet saturated air, P_0 : 15 psia

Total Operation time, Θ : 3.5 hr.

Temperature and pressure distribution

Distance, x/L	Temperature, $\frac{T - T_0}{T_0 - t_L}$	Pressure, $\frac{P}{P_0}$
0	0	1.0
0.166	0.0013	0.855
0.333	0.015	0.70
0.50	0.005	0.48
0.667	-0.026	0.36
0.833	-0.205	0.22
1.0	-1.0	0

Moisture distribution

Layer, x	0-0.05	0.5-1.0	1.0-1.5	1.5-2.0	2.0-2.5	2.5-3.0
% of moisture content by dry weight	0.24	0.135	0.23	1.05	9.86	12.67

Experiment B

Porous material: Fine glass beads

Bulk density, ρ_s: 94 lb/ft^3

Length of porous column, L : 1 inch

Mass flow rate of dry air, G: 23.4 lb/ft^2-hr

Thermal conductivity of the dry porous bed, K: 0.117 BTU/ft-F-hr

Temperature of inlet saturated air, T_0 : 79.7°F

Temperature of solid particles at x = L, t_L : 64°F

Pressure of inlet saturated air, P_0 : 16.2 psia

Total operation time, Θ: 2.0 hr

Temperature and pressure distribution

Distance, x/L	Temperature, $\frac{T-T_0}{T_0-t_L}$	Pressure, $\frac{P}{P_0}$
0	0	1.0
0.25	-0.017	
0.50	-0.08	0.555
0.75	-0.35	
0.85		0.165
1.0	-1.0	0

Moisture distribution

Layer, x	0 - 0.33	0.33-0.67	0.67-1.0
% or moisture content by dry weight	1.04	1.38	9.13

Experiment C

Porous material: Mixture of 2/3 fine glass beads and 1/3 chrome powder by weight

Bulk density, ρ_s : 116 lb/ft^3

Length of porous column, L: 1 inch

Mass flow rate of dry air, G : 23.9 lb/ft^2-hr

Thermal conductivity of the dry porous bed, K: 0.15 BTU/ft-F-hr

Temperature of inlet saturated air, T_0 : 78.7°F

Temperature of solid particles at x = L, t_L : 61.7°F

Pressure of inlet saturated air, P_0 : 16.7 psia

Total operation time, Θ: 1.5 hr

Temperature and pressure distribution

Distance, x/L	Temperature $\frac{T-T_0}{T_o-t_L}$	Pressure, $\frac{P}{P_o}$
0	0	1
0.313	-0.04	
0.5		0.6
0.688	-0.245	
0.813	-0.375	
1.0	-1.0	0

Moisture distribution

Layer, x	0-0.25	0.25-0.50	0.50-0.75	0.75-1.0
% of moisture content by dry weight	0.083	0.067	0.146	5.84

Experiment D

Porous material: Mixture of 1/3 fine glass beads and 2/3 chrome powder by weight

Bulk density, ρ_s : 151 lb/ft^3

Length of porous column, L: 1 inch

Mass flow rate of dry air, G: 23.3 lb/ft^2-hr

Thermal conductivity of the dry porous bed, K: 0.2 BTU/ft-F-hr

Temperature of inlet saturated air, T_0 : 79° F

Temperature of solid particles at x = L, t_L : 61.5°F

Pressure of inlet saturated air, P_0 : 16.6 psia

Total operation time, Θ : 2 hr

Temperature and pressure distribution

Distance, x/L	Temperature, $\frac{T-T_0}{T_0-t_L}$	Pressure $\frac{P}{P_0}$
0	0	1.0
0.25	-0.084	
0.5		0.55
0.625	-0.404	
0.75	-0.56	
1.0	-1.0	0

Moisture distribution

Layer, x	0-0.25	0.25-0.50	0.50-0.75	0.75-1.0
% of moisture content by dry weight	1.4	1.0	2.4	4.0

Experiment E

Porous material: Sandy soil

Bulk density, ρ_s: 100 lb/ft^3

Length of porous column, L: 1 inch

Mass flow rate of dry air, G: 23 lb/ft^2-hr

Thermal conductivity of the dry porous bed, K: 0.218 BTU/ft-F-hr

Temperature of inlet saturated air, T_0 : 81.5°F

Temperature of solid particles at x = L, t_L : 63.5° F

Pressure of inlet saturated air, P_0: 16.22 psia

Total operation time, ϑ: 1.75 hr

Temperature and pressure distribution

Distance, x/L	Temperature, $\frac{T-T_0}{T_0-t_L}$	Pressure, $\frac{P}{P_0}$
0	0	1.0
0.25	0.0170	
0.50	-0.0921	0.5
0.75	-0.3114	
1.00	-1.0	0

Moisture distribution

Layer, x	0 - 0.33	0.33-0.67	0.67-1.0
% of moisture content by dry weight	2.06	3.13	8.38

Experiment F *

Porous material: Sandy soil with stainless steel pins

Bulk density, ρ_s : 151 lb/ft^3

Length of porous column, L: 1.5 inches

Mass flow rate of dry air, G: 8.1 lb/ft^2-hr

Thermal conductivity of the dry porous bed, K: 2.1 BTU/ft-hr-°F

Temperature of inlet saturated air, T_0 : 69.5°F

Temperature of solid particles at x = L, t_L: 56.4°F

Pressure of inlet saturated air, P_0 : 14.94 psia

Total operation time, Θ: 10 hr

Temperature and pressure distribution

Distance, x/L	Temperature $\frac{T-T_0}{T_0-t_L}$	Pressure $\frac{P}{P_0}$
0	1	1
0.33	-0.244	
0.67	-0.61	0.35
0.88	-0.848	
1.0	-1.0	0

Moisture distribution

Layer, x	0-0.167	0.167-0.333	0.333-0.5	0.5-0.667	0.667-0.834	0.834-1.0
% of moisture content by dry weight	3.71	3.56	3.59	3.56	3.64	3.82

* Ref. 10, p. 68